2-1-2018

Fully Probabilistic Analysis of FRP-to-Concrete Bonded Joints Considering Model Uncertainty

Dongming Zhang
Tongji University

Xiang-Lin Gu
Tongji University

Qian-Qian Yu
Tongji University

Hongwei Huang
Tongji University

Baolin Wan
Marquette University, baolin.wan@marquette.edu

See next page for additional authors

Accepted version. *Composite Structures*, Vol. 185 (February 1, 2018): 786-806. DOI.

Fully Probabilistic Analysis of FRP-to-Concrete Bonded Joints Considering Model Uncertainty

Dongming Zhang
Department of Geotechnical Engineering, Tongji University, No. 1239 Siping Road, Shanghai 200092, China
Xiang-Lin Gu
State Key Laboratory for Disaster Reduction in Civil Engineering, Tongji University, Shanghai 200092, China
Department of Structural Engineering, Tongji University, No. 1239 Siping Road, Shanghai 200092, China
Qian-Qian Yu
State Key Laboratory for Disaster Reduction in Civil Engineering, Tongji University, Shanghai 200092, China
Department of Structural Engineering, Tongji University, No. 1239 Siping Road, Shanghai 200092, China
Hongwei Huang
Department of Geotechnical Engineering, Tongji University, No. 1239 Siping Road, Shanghai 200092, China
Baolin Wan
Department of Civil and Environmental Engineering, Marquette University, Milwaukee, WI
Cheng Jiang
Department of Civil and Environmental Engineering, The Hong Kong Polytechnic University, Hong Kong Special Administrative Region

Abstract

This work presents a full reliability-based analysis framework for fiber-reinforced polymer (FRP)-to-concrete bonded joints considering model uncertainty. Eight frequently used bond strength models for FRP-to-concrete bonded joints were calibrated by defining a model factor. A total of 641 well-documented tests were considered. Four of the eight models had model factors that correlated with input design parameters and the systematic part of the model factor was removed by a regression equation *f*. By doing this type of characterization, all eight model factors could be comparatively uniform and described by lognormally distributed random variables. The merit of the uniform model uncertainties after calibration for the eight models was established by the reliability analysis. This study improves the predictability of concrete strengthened with fiber composites and provides useful suggestions on their model uncertainties in engineering practice.

Keywords

FRP-to-concrete, Bond strength, Reliability analysis, Model uncertainty, Multiple regression analysis

1. Introduction

External bonding with fiber-reinforced polymer (FRP) composite materials has been recognized as an alternative to conventional techniques for strengthening aged reinforced concrete (RC)[1,2,3,4,5,6,7,8,9] and steel structures.[10,11,12,13,14,15,16] FRP materials have advantages of high strength-to-weight ratio, good resistance to corrosion and ease of installation. For systems relying on load transfer between FRP and substrate, the utilization of FRP's mechanical properties largely depends on their interfacial bond behavior. Extensive experimental studies have been performed to investigate FRP-to-concrete interfacial behavior, and a typical set-up of a single shear pull-out test is schematically displayed in Fig. 1. Numerous models have been proposed to predict the bond strength of FRP-to-concrete bonded joints,[17,18,19,20,21,22,23,24] as well as bond-slip models between FRP and concrete.[22,25,26,27,28,29,30,31,32]

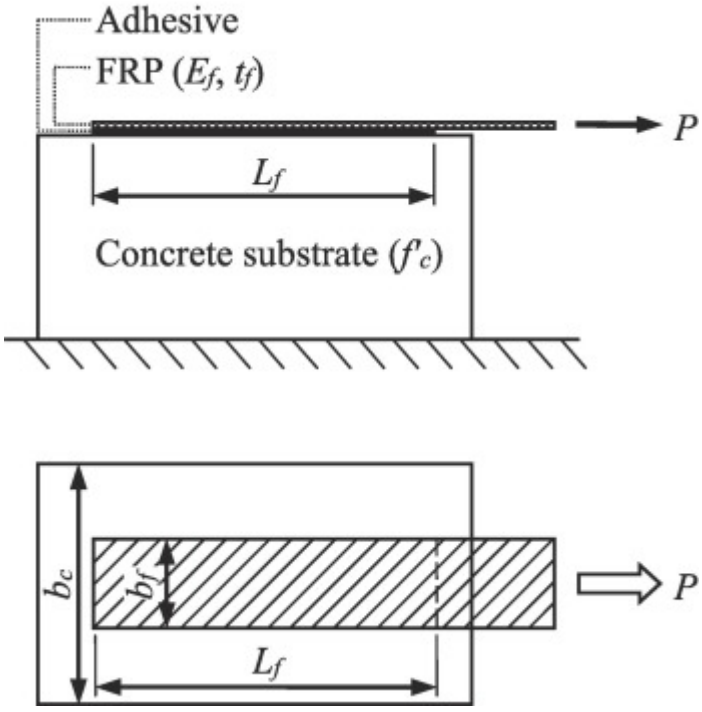

Fig. 1. Schematic diagram of a single shear pull-out test.

The overall mechanical performance of the FRP-to-concrete bonded joints largely depends on material properties (i.e., FRP, concrete and adhesive), preparation of concrete surface, and workers' skill of applying FRP to concrete substrate. Note that all the above sources inevitably contain uncertainties. The uncertainties either in engineering prediction or in manufacturing process can be partially addressed by the reliability-based design (RBD).[33] Hence, the RBD framework for FRP strengthening of concrete structures has been well studied in the past few decades. Plevris et al.[34] first presented a reliability-based analysis procedure, which considered the uncertainty of carbon FRP (CFRP) laminates in flexurally retrofitted concrete beams. Later, the calibration of statistical characteristics in input parameters of FRP was presented by many researchers.[35,36,37,38] Moreover, the RBD procedure has been recognized by both American Concrete Institute (ACI) and American Association of State Highway and Transportation (AASHTO) as guidelines of FRP system for RCs.[39,40]

In the resistance factor approach, it is common practice to introduce a reduction factor ψ for the structural resistance to reach a required reliability index β. Due to various model uncertainties obtained by different models, each model is associated with a specific value of ψ, when targeting at a certain reliability level. Recently, Shi et al.[37] summarized six flexural strength prediction models of FRP-strengthened concrete beams with intermediate crack-induced debonding failure and derived the reduction factor for each model. It was interesting to find that the values of factor ψ were quite different among these six models, ranging from 0.2 to 0.8. Thus, it is highly desirable if the variation of the reduction factor ψ can be removed to obtain a uniform ψ without losing the required level of reliability for all models.

The presence of different magnitudes of ψ should be attributed to the predictability of each model. Each prediction model has its own assumptions and limitations, which cause difference from the reality of the world,[41] resulting in a model uncertainty. Hence, the model uncertainty plays an important role in the calibrated reduction factor ψ. To be more specific, different models produce different levels of model uncertainties and thus result in different reduction factors.

For flexural members strengthened with externally bonded FRP materials, the contribution of FRP on the flexural bearing capacity is dependent on the bond strength between FRP and concrete, which is normally evaluated by a shear pull-out test of FRP-to-concrete bonded joints. Therefore, uncertainties of the bond behavior of these joints are of great concern to those models implementing RBD for FRP retrofitted concrete beams. A thorough literature survey by the authors revealed little information on how to calibrate model uncertainties of so many existing FRP-to-concrete bond strength models. The aim of this paper is to present an approach for calibrating the uncertainties of existing FRP-to-concrete bond strength models. In order to quantify the uncertainty of a model, it is customary to define a model factor defined by the ratio of a measured value to a predicted value. The measured value can be obtained either from physical tests or from field case, and the predicted value is calculated by the models. By using this method, a typical range of the model factor is obtained for a specific problem configuration. This range of values and its associated frequency histogram can then be modeled by a random variable. The only requirement of using this approach is that the values must be "random" and should not depend on input parameters.

For some FRP-to-concrete bond strength models, the calculated model factor is found to be correlated with input parameters, which conflicts with the basic definition of the model factor. This conflict is the possible reason for different reduction factors in the models summarized by Shi et al.[37] Therefore, regression or other methods are needed to remove the systematic effect from input parameters, and the regression residual must be checked for randomness. This approach to characterizing model factors has been explained by Zhang et al.,[42] and it was adopted in this paper.

Based on this type of systematic calibration, variation of the reduction factor ψ for different models is reduced to a uniform value targeting at a certain reliability index β. In this way, the design of FRP-to-concrete bonded joints from the reliability perspective could be uniform regardless of the specific model that is adopted in

practice. In total, 641 FRP-to-concrete shear pull-out test results were collected with well-documented test parameters. Eight frequently used bond strength models, i.e., presented by Van Gemert,[17] Holzenkämpfer,[18] Hiroyuki and Wu,[19] Chen and Teng,[20] *fib*,[21] Dai et al.,[22] Zhou[23] and Wu and Jiang,[24] were incorporated in this paper to calibrate the model uncertainties. The randomness of these eight model factors was carefully checked. Four of the models had a systematic model factor that was dependent on the input test parameters. Hence, a multiple regression analysis was carried out by using 501 data points from the test data set. The systematic part of the model factor was removed by a regressed equation using the five input parameters. Then, the randomness of the residual model factor was verified by using the remaining 140 data points. Case studies were presented herein on the FRP-to-concrete bonded joints with respect to the full reliability analysis and RBD application. These case studies were summarized based on the calibrated model uncertainties presented in this paper. Therefore, the calculated uniform reliability level and the consistent joint designs for all the eight models were validated. The proposed framework of calibration of the model factor is helpful in the practice of reliability analysis to obtain a uniform model uncertainty, and consequently a desirable reliability level.

2. Bond strength models

Numerous models have been developed to predict the interfacial bond strength. The bond strength in this paper is defined as the peak load in pull-out tests.[20] Eight frequently used models are selected in this study. They were proposed by Van Gemert,[17] Holzenkämpfer,[18] Hiroyuki and Wu,[19] Chen and Teng,[20] *fib*,[21] Dai et al.,[22] Zhou[23] and Wu and Jiang[24] as shown in Table 1 and are referred in short as the VG Model, HO Model, HW Model, CT Model, *fib* Model, Dai Model, Zhou Model and WJ Model, respectively, in the remainder of this paper. These models are either empirical models purely based on experimental results, or semi-empirical models involving fracture mechanics theory and test results. In the table, P_u is the peak load (bond strength), E_f is the elastic modulus of FRP material, t_f is the thickness of FRP material, b_f is the width of FRP material, b_c is the width of concrete substrate, f_{cu} is the concrete cubic compressive strength, f'_c is the concrete cylinder compressive strength ($f_c' = 0.78f_{cu}$), f_t is the concrete tensile strength ($f_t = 0.395(f_c'/0.78)^{0.55}$), L_f is the bond length, L_e is the effective bond length, κ_w is the coefficient of bond width ratio, τ_a is the bond stress, and G_f is the interfacial fracture energy, and c_f, k_c, c_1, c_2, α, and Δb_f are constants.

Table 1. Selected pull-out bond strength models.

Reference	Model
Van Gemert (1980)	$P_u = 0.5 b_f L_f f_t$
Holzenkämpfer (1994)	$G_f = c_f f_t, c_f = 0.204\text{mm}, P_u = b_f \sqrt{G_f E_f t_f}$
Hiroyuki and Wu (1997)	$\tau_a = 5.88 {L_f}^{-0.669}, P_u = \tau_a b_f L_f$
Chen and Teng (2001)	$L_e = \sqrt{\frac{E_f t_f}{\sqrt{f_c'}}}, \kappa_w = \sqrt{\frac{2 - b_f/b_c}{1 + b_f/b_c}}$ $P_u = \begin{cases} 0.427 \kappa_w b_f L_e \sqrt{f_c'} \text{ if} L_f \geqslant L_e \\ 0.427 \kappa_w b_f L_e \sqrt{f_c'} \sin\frac{\pi L_f}{2L_e} \text{ if} L_f < L_e \end{cases}$

Reference	Model
fib (2001)	$L_e = \sqrt{\frac{E_f t_f}{c_2 f_t}}, \kappa_w = 1.06\sqrt{\frac{2-\frac{b_f}{b_c}}{1+\frac{b_f}{400}}} \geqslant 1 (b_f/b_c \geqslant 0.33)$ $P_u = \begin{cases} \alpha c_1 k_c \kappa_w b_f \sqrt{E_f t_f f_t} \text{ if} L_f \geqslant L_e \\ \alpha c_1 k_c \kappa_w b_f \sqrt{E_f t_f f_t}\frac{L_f}{L_e}\left(2-\frac{L_f}{L_e}\right) \text{ if} L_f < L_e \end{cases}$ $k_c = 1.0$, $c_1 = 0.64$, $c_2 = 2$, α=0.9, E_f in MPa
Dai et al. (2005)	$G_f = 0.514 f_c'^{0.236}, \Delta b_f = 3.7\text{mm}$ $P_u = \begin{cases} (b_f + 2\Delta b_f)\sqrt{2E_f t_f G_f} \text{ if} b_f \geqslant 100\text{mm} \\ b_f \sqrt{2E_f t_f G_f} \text{ if} b_f < 100\text{mm} \end{cases}$
Zhou (2009)	$L_e = 1.6841\sqrt{\frac{E_f t_f}{f_c^{2/3}}}, \kappa_w = \sqrt{\frac{2.9-\frac{b_f}{b_c}}{0.6+\frac{b_f}{b_c}}}, G_f = 0.0498\kappa_w^2\sqrt{f_{cu}},$ $P_u = \begin{cases} b_f\sqrt{2E_f t_f G_f} \text{ if} L_f \geqslant L_e \\ b_f\sqrt{2E_f t_f G_f}\frac{L_f}{L_e}(2-\frac{L_f}{L_e}) \text{ if} L_f < L_e \end{cases}$
Wu and Jiang (2013)	$\lambda = 1 + 0.222 f_c'^{0.304}$, $\kappa_w = \lambda + (1-\lambda) b_f/b_c$, $\alpha = 0.094 f_c'^{0.026}$, $\beta = \frac{0.134 E_f t_f^{0.5}}{\kappa_w f_c'^{0.082}}$, $\eta = -3.61 e^{-0.4454\frac{L_f}{\beta}} + 4.11 e^{-0.3835\frac{L_f}{\beta}}$, $P_u = \frac{\alpha E_f t_f b_f \eta \sqrt{1-\eta^2}\sinh(\sqrt{1-\eta^2}L_f/\beta)}{\beta[1+\eta\cosh(\sqrt{1-\eta^2}L_f/\beta)]}$

Early models, e.g., the VG Model in 1980, used fewer parameters than more recent models, such as the WJ Model in 2013. This is consistent with the advancement of knowledge about the performance of FRP-to-concrete bonded joints in past three decades. However, this does not mean that the prediction by earlier models is not as accurate as those presented in recent models. The earlier models might be more frequently used by practitioners since they might be more convenient and their discoveries could offer more insight into key parameters. Hence, it is of great necessity to present an analysis of the model uncertainties for those frequently used models to reduce the additional uncertainty or bias induced by the choice of specific models in the RBD.

3. Collection of database

It is believed that the bond strength of a FRP-to-concrete bonded jointcould be affected by many factors, e.g., FRP-related and concrete-related material properties. However, it is not practical to incorporate all the possible factors in this paper to evaluate the model uncertainty. Among all the factors, five parameters are singled out as the most significant: 1) FRP elastic modulus E_f, 2) FRP thickness t_f, 3) bond length L_f, 4) FRP-to-concrete width

ratio b_f/b_c, and 5) concrete cylinder compressive strength f'_c.[1,20,29,43,44,45,46] Hence, they are the key parameters studied in this paper. To adequately cover these five parameters and the associated bond strength P_u, a state-of-the-art database was collected from the literature.[22,23,24,25,43,47,48,49,50,51,52,53,54,55,56,57,58,59,60,61,62,63,64,65,66,67,68,69,70,71,72,73,74,75,76,77,78] (Detailed references can be referred in Table 2 and are not listed here due to space constraints and to keep the focus on the most important aspects of this study). For pull-out tests on externally bonded FRP joints, failure with a thin layer of concrete being pull-off from the concrete substrate is considered as desirable and representing an adequate bond quality of the specimens. Therefore, cases with this kind of failure mode were strictly selected for analysis in this present study. Tests with a soft adhesive or a thick adhesive layer were excluded from the database because they can produce significantly different bond properties than those meeting the expected (accepted) consistency.[22,24,29,53] It should also be pointed out that, only single/double shear pull-out tests were included while bending tests were excluded here. A total of 641 test results were extracted and are listed in Table 2, with the FRP elastic modulus E_f ranging from 22.5 to 390.0 GPa, the FRP thickness t_f ranging from 0.08 to 4.00 mm, the bond length L_f ranging from 20 to 406 mm, the FRP-to-concrete width ratio b_f/b_c ranging from 0.10 to 1.00, and the concrete cylinder compressive strength f'_c ranging from 17.0 to 75.5 MPa. With respect to the fiber type, CFRP, aramid FRP (AFRP), glass FRP (GFRP), basalt FRP (BFRP), and graphite FRP are all included.

Table 2. Outline of database.

Reference	Number of tests	FRP material	E_f (GPa)	t_f (mm)	L_f (mm)	b_f/b_c	f'_c (MPa)
Meada et al. (1997)	4	CFRP	230.0	0.11–0.22	75–300	0.50	40.8–43.3
Taljsten, B. (1997)	4	CFRP	170.0	1.25	100–400	0.25	50.1–59.9
Bizindavyi and Nwale (1999)	4	CFRP/GFRP	29.2–75.7	0.33–2.00	160–320	0.17	42.5
Brosens and Gemert (1999)	23	CFRP	235.0	0.17–0.50	150–200	0.53–0.80	43.7
Kamiharako et al. (1999)	11	CFRP/AFRP	80.0–270.0	0.11–0.22	100–250	0.20–0.90	34.9–75.5
Wu et al. (2001)	18	CFRP/AFRP	23.9–390.0	0.08–1.00	250–300	0.40–1.00	42.0–57.6
Dai et al. (2002)	16	CFRP/GFRP/AFRP	74.0–230.0	0.11–0.762	210–330	0.25	33.1–35.0
Dai (2003)	17	CFRP	230.0	0.11–0.33	20–300	0.13–0.25	32.8–35.0
Zhao and Ansari (2004)	6	CFRP	73.1	1.00	80–160	0.39	38.8
Dai et al. (2005)	20	CFRP/AFRP/GFRP	74.0–230.0	0.11–1.14	330	0.25	35.0
Mazzotti et al. (2005)	4	CFRP	165.0	1.20	50–400	0.33	52.6
Yao et al. (2005)	56	CFRP/GFRP	22.5–256.0	0.17–1.27	75–240	0.10–0.67	18.9–27.1
Sharma et al. (2006)	24	CFRP/GFRP	32.7–300.0	1.20–4.00	100–300	0.30–0.50	29.7–35.8

Reference	Number of tests	FRP material	E_f (GPa)	t_f (mm)	L_f (mm)	b_f/b_c	f'_c (MPa)
Toutanji et al. (2007)	2	CFRP	110.0	0.50–0.66	100	0.25	17.0
Leone et al. (2009)	3	CFRP/GFRP	73.0–225.6	0.12–1.00	300	0.67	32.1
Zhou (2009)	123	CFRP/GFRP	71.0–237.0	0.11–0.34	20–200	0.10–1.00	45.6–65.4
Ceroni and Pecce (2010)	17	CFRP	230.0	0.17–0.33	150	0.17–0.67	28.1
Shi et al. (2010)	12	CFRP/BFRP	81.5–239.8	0.11–0.42	230	0.50	27.1
Bilotta et al. (2011)	11	CFRP	141.0–221.0	1.20–1.70	300	0.38–0.63	19.0
Biolzi et al. (2013)	6	CFRP	170.0	1.40	30–250	0.33	32.6
Wu and Jiang (2013)	65	CFRP	238.1–248.3	0.17–0.50	30–400	0.33	25.3–59.0
Diab and Farghal (2014)	1	CFRP	230.0	0.17	250	0.50	40.0
Hosseini and Mostofinejad (2014)	22	CFRP	238.0	0.13	20–250	0.32	30.0
Ko et al. (2014)	14	CFRP	165.0–210.0	1.00–1.40	300	0.40–0.67	27.7–31.4
Zhang et al. (2014)	4	BFRP	37.1–39.5	1.48–1.51	200	0.48–0.50	40.9–46.4
Kalfat and Al-Mahaidi (2015)	2	N/A	195.0	2.80	370	0.25	28.7
Mohammadi and Wan (2015)	4	N/A	155.0	1.50	406	0.33	33.0
Pan et al. (2015)	4	CFRP	150.8	1.30	170	0.25	37.4
Zhou et al. (2015)	2	CFRP/GFRP	89.3–240.0	0.17–0.17	300	0.50	43.8
Ceroni et al. (2016)	2	CFRP	170.0	1.40	350	0.31	19.0
Calibration data set	***501***		***22.5–390.0***	***0.08–4.00***	***20–406***	***0.10–1.00***	***17.0–75.5***
Chajes et al. (1996)	15	Graphite FRP	108.5	1.02	51–203	0.11–0.17	24.0–47.1
Takeo et al. (1997)	29	CFRP	230.0–373.0	0.11–0.50	100–300	0.40	24.1–49.3
Sato et al. (2000)	14	CFRP	230.0–372.0	0.11–0.55	75–300	0.20–0.67	23.8–45.9

Reference	Number of tests	FRP material	E_f (GPa)	t_f (mm)	L_f (mm)	b_f/b_c	f'_c (MPa)
Nakaba et al. (2001)	16	CFRP/AFRP	124.5–261.1	0.08–0.33	300	0.50	23.8–57.6
Ebead et al. (2004)	32	CFRP/GFRP	29.2–75.7	0.33–2.00	50–320	0.17	42.5
Pham and Al-mahaidi (2004)	16	CFRP	209.0	0.35	60–220	0.71	55.6
Zhu et al. (2014)	18	BFRP/CFRP	81.5–239.8	0.11–0.42	230	0.50	32.1
Verification data set	***140***		***29.2–373.0***	***0.084–2.00***	***50–320***	***0.11–0.71***	***23.8–57.6***
Total	***641***		***22.5–390.0***	***0.08–4.00***	***20–406***	***0.10–1.00***	***17.0–75.5***
Mean			***190.7***	***0.47***	***166***	***0.39***	***38.7***
COV			***0.40***	***1.19***	***0.59***	***0.50***	***0.31***

Note:

1. Researchers who would like to get access to the database, please contact the authors.
2. In some references, the detailed type of FRP is not given, and these cases are indicated as “N/A” in the column of “FRP material”.

4. Model uncertainty of bond strength

Because all calculation methods involve varying degrees of idealization, model uncertainty always exists. The multiplicative model is commonly adopted to define a model factor[79,80]

(1) $P_u^m = \varepsilon \times P_u^c$

where P_u^m is the experimentally measured bond strength collected in the database, P_u^c is the calculated bond strength obtained from the prediction models, and ε is the model factor, which is associated with a specific prediction model based on Eq. (1). When the model factor is larger than one, it indicates that the calculated strength is smaller than the measured value and vice versa. Theoretically speaking, the closer the mean value of ε approaches to one, the more accurate the model is. The smaller the coefficient of variance (COV) of ε is, the more precise the model is. However, ε larger than one is considered to be conservative from the practical point of view, while ε smaller than one is not safe. With the 641 pull-out tests, 641 calculated P_u^c and the associated model factor ε by using Eq. (1) could be obtained for each prediction model, as shown in Table 1. Fig. 2 plots the comparison between the calculated ultimate load P_u^c (vertical axis) and the tested ultimate load P_u^m (horizontal axis) of the 641 data points for all the eight models. It is shown in Fig. 2 that for the CT Model, *fib* Model, Zhou Model and WJ Model, the data points are closely located around the 45-degree line (i.e., a line for $P_u^c = P_u^m$). However, for the predictions obtained from the other models, the data points are either sparsely distributed around the 45-degree line, as shown in Fig. 2(e) (the VG Model) or closely distributed around a line that is not the 45-degree line, as shown in Fig. 2(f), (g) and (h) (the HO Model, HW Model and Dai Model).

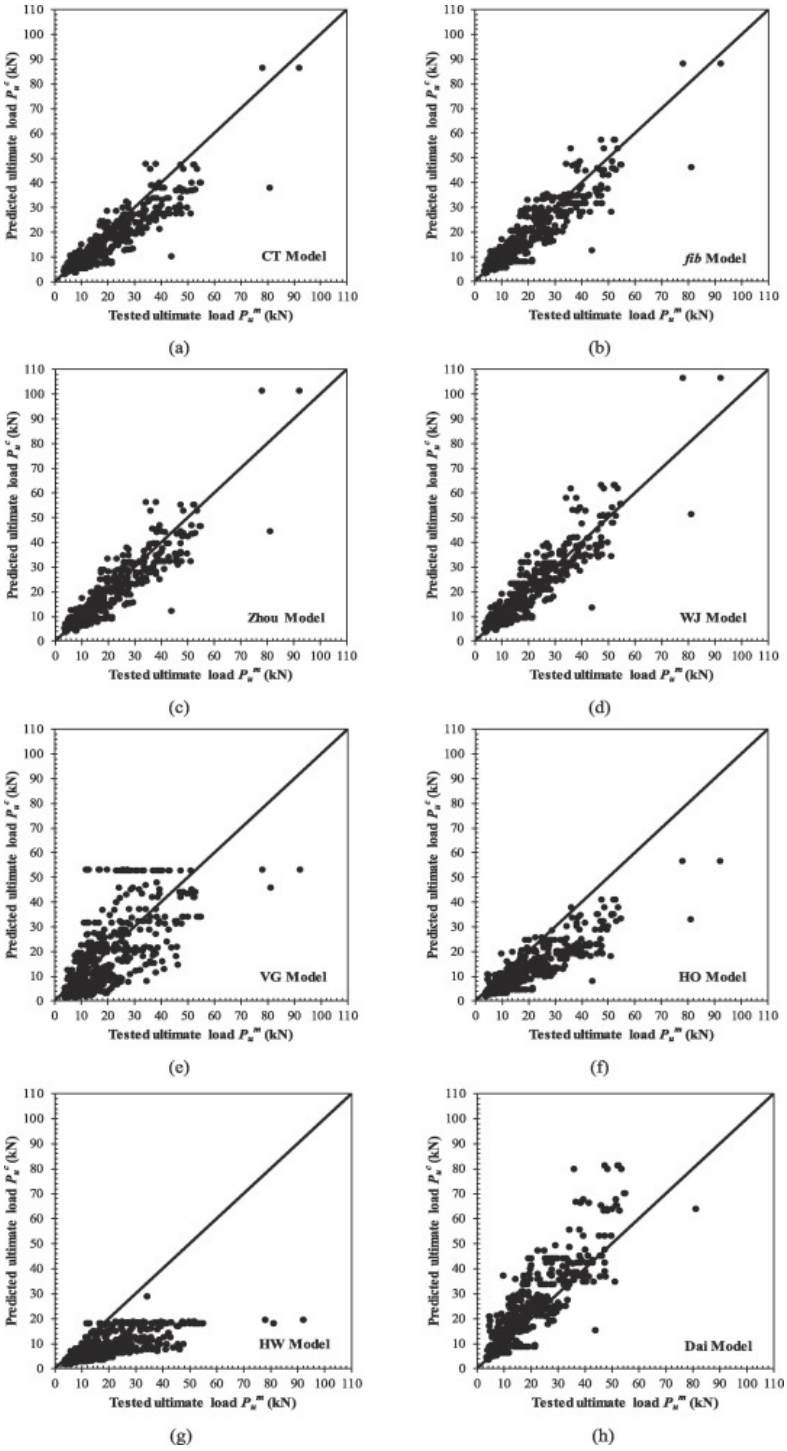

Fig. 2. Comparison between predicted ultimate load and tested ultimate load for the eight models: (a) CT Model, (b) *fib* Model, (c) Zhou Model, (d) WJ Model, (e) VG Model, (f) HO Model, (g) HW Model and (h) Dai Model.

Fig. 3 plots a histogram of the 641 calculated ε. The mean value of εranges from 0.86 (the Dai Model) to 2.24 (the HW Model). Based on averaging, the prediction by the Dai Model is larger than the measured strength, while the prediction by the HW Model is much smaller than the experimental results. It is observed from Fig. 3 that the COV of ε ranges from 0.27 (the CT Model, WJ Model and Zhou Model) to 0.66 (the VG Model). It is common for a model factor to have a COV with a range from 0.2 to 0.[3.37,42,79] However, for those models with an extremely high COV, such as the COV of the VG Model equal to 0.66 as shown in Fig. 3, a closer look at the systematic reason causing the large variance in the prediction is necessary. In other words, the randomness of

the model factor ε directly obtained from Eq. (1) should be checked before the characterization of the model uncertainty. A graphical verification of the randomness of the model factor for the VG Model (referred to as ε_{VG} hereafter) against the bond length L_f of FRP is plotted in Fig. 4, where a nonlinear negative trend can be clearly observed. It is implied that the calculated ε directly from Eq. (1) using the 641 test results might not be a random variable but has a strong dependency on the input parameter, i.e., the bond length L_f in this case. A detailed Spearman correlation analysis was carried out for the model factor ε_{VG} with five design parameters for the 641 cases. The Spearman correlation analysis is a non-parameter test with a null hypothesis of zero-rank (Spearman) correlation if the significance level is larger than 5%. However, the correlation between the model factor ε_{VG} of the VG Model and most of the five parameters has a high level of R with an extremely low level of p-value as shown in the second and fourth columns in Table 3. It statistically proves a systematic dependency for ε_{VG} on the design parameters. One may question whether the parameter correlation for the model factor ε_{VG} is due to ignoring the effects of parameters t_f, E_f and b_c on the calculated P_u^c since the VG Model does not incorporate these parameters, as shown in Table 1. A similar statistical analysis for checking the randomness of ε_{Dai} for the Dai Model incorporating more parameters was also conducted, and the results of the correlation coefficient R and significance p-value are also given in Table 3. The sixth and eighth columns apparently confirm that ε_{Dai} is correlated with four parameters (i.e., E_f, t_f, L_f and b_f/b_c) with p-values much less than the customary 5% level of significance. A similar procedure was performed for the HO Model and HW Model. It was demonstrated that for the four models with a COV higher than 0.3, i.e., the VG Model, HO Model, HW Model and Dai Model, the dependency on the input parameters is statistically significant (for simplicity, statistics for the HO Model and HW Model are not listed in Table 3), and a more detailed study of the dependency is required.

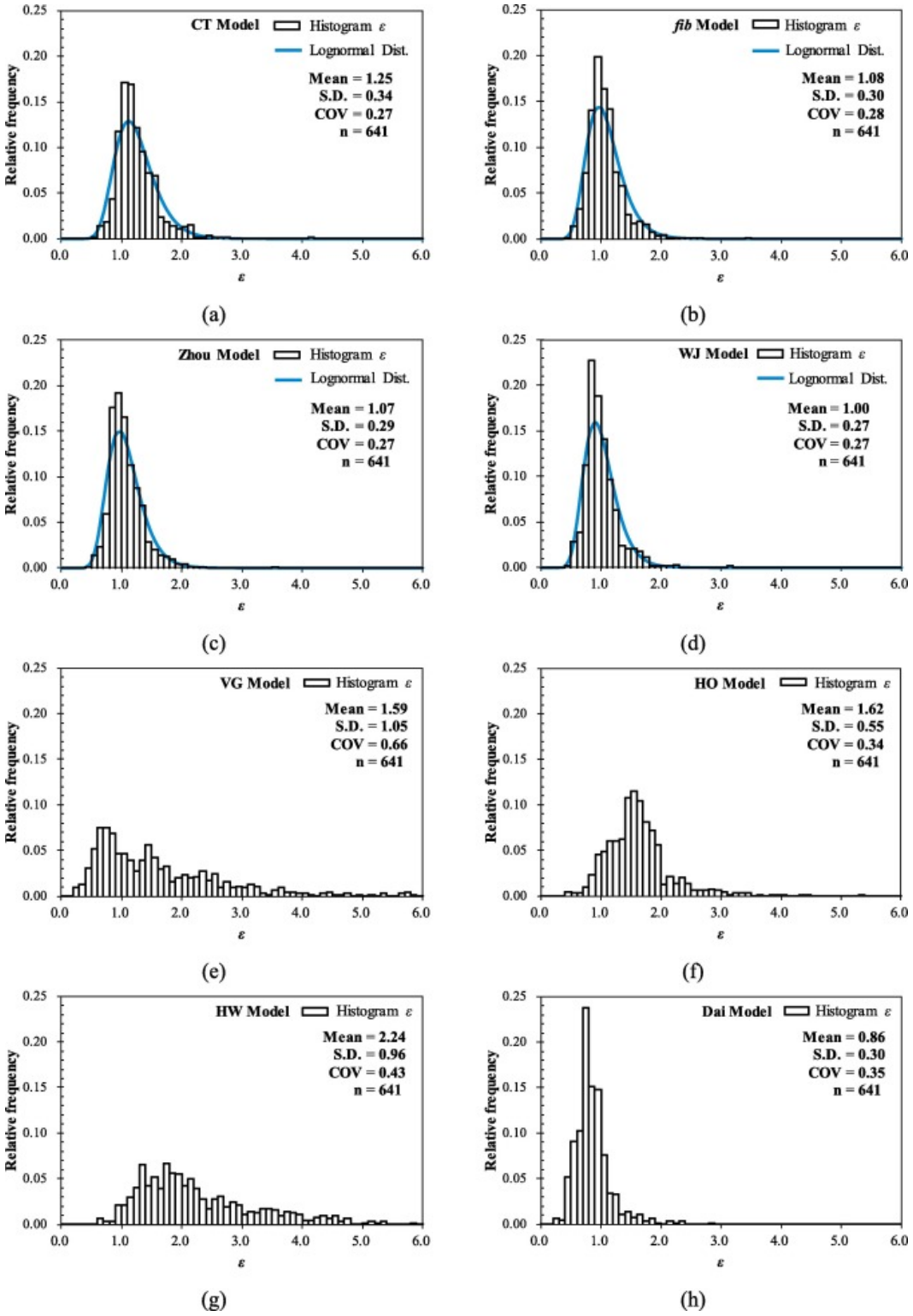

Fig. 3. Histograms of ε of 641 data points for the eight models: (a) CT Model, (b) *fib* Model, (c) Zhou Model, (d) WJ Model, (e) VG Model, (f) HO Model, (g) HW Model and (h) Dai Model.

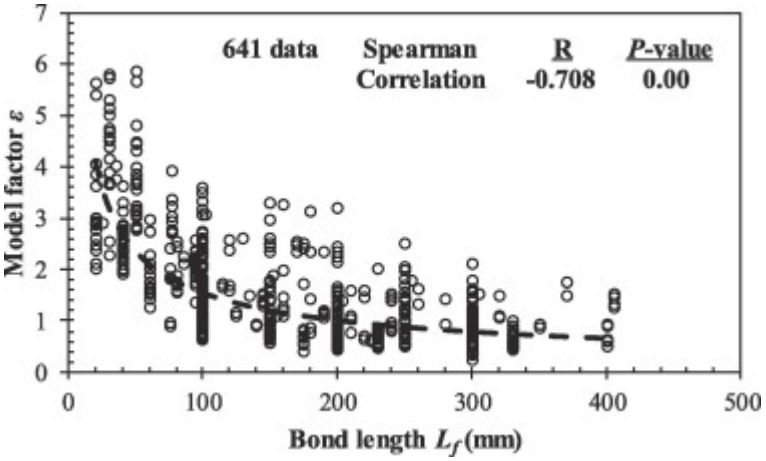

Fig. 4. The model factor ε against bond length L_f (VG Model).

Table 3. Dependency check of the model factor on input parameters for the VG Model and Dai Model.

Parameter	VG Model				Dai Model			
	Correlation coefficient *R*		Significance *p*-value		Correlation coefficient *R*		Significance *p*-value	
	Before ε	After ε^*	Before ε	After ε^*	Before ε	After ε^*	Before ε	After ε^*
E_f	0.134	0.045	0.001	0.255	−0.132	0.051	0.001	0.199
t_f	0.246	0.101	0.000	0.010	0.12	0.026	0.002	0.515
L_f	−0.708	−0.051	0.000	0.198	0.441	0.136	0.000	0.001
b_f/b_c	−0.295	−0.069	0.000	0.081	−0.324	0.008	0.000	0.839
f'_c	−0.062	−0.011	0.118	0.773	0.030	−0.062	0.453	0.116

Since the 641 tests have covered frequently used ranges of parameters for designs of FRP-to-concrete bonded joints, a regression analysis can be applied to remove the dependency of the model factor on the parameters. The systematic correlation of the model factor with the input parameters could be represented by a regression equation *f*. However, the model factor ε cannot be identically equal to the correlated part represented by regression equation *f*. The residual ε^*after removing the correlation part (represented by equation *f*) from the model factor ε always exists. Hence, the model factor ε can be decomposed into a systematic part that is determined by the regression equation *f* and a residual random factor ε^*:

(2) $\varepsilon = f \times \varepsilon^*$

Substituting Eq. (2) into Eq. (1) yields

(3) $P_u^m = f \times \varepsilon^* \times P_u^c$

Hence, for the four models with a large COV, the remaining work for characterizing the model factor is to reduce its COV by establishing an appropriate regression equation *f* and subsequently characterizing the residual random factor ε^*.

5. Test data based regression analysis

In total, 501 data points were selected to build the regression equation (see the first 30 rows in Table 1), while the remaining 140 data points (see the latter rows in Table 1) were used to verify the accuracy of the regression

equation and the associated model factor. With respect to the selection criteria of the data set, first, the data of one reference was kept together for the convenience of presentation; second, the calibration and verification data sets should cover the distribution range of all the parameters as much as possible. Based on these two requirements, the data from 37 references was arbitrarily selected to compose the calibration data set (501 points) and the verification data set (140 points). This is because the accuracy of a regression equation largely depends on the parameter range for regression, which could affect the results of verification. Four models need to be calibrated, but only the VG Model is discussed in detail to maintain the focus and space constraints of the paper. Similar procedures can be followed for the other models and the results of regression are given at the end of this section.

Since it is a multiple regression analysis, the regression is performed through two steps. The first step is to identify the correlation function type (i.e., core function) of the model factor with each of the five input parameters. In the calibration data set, when a specific value of a test parameter is selected, there might be more than one test case. For these test cases with a specific parameter that matches in value, other parameters might have different values from each other. To remove the multi-parameter effect on the calculated model factor and to capture the true relationship between the interested parameter and the model factor, an averaging treatment of the model factor was adopted in the first step of regression, which is frequently performed in similar work with multiple regression analysis involved.[42,81,82] For example, given the concrete cylinder compressive strength f'_c at 17 MPa, there are two cases with the following parameters:

(1)

$$f'_c = 17 \text{ MPa}, E_f = 110 \text{ GPa}, t_f = 0.495 \text{ mm}, L_f = 100 \text{ mm}, b_f/b_c = 0.25, \varepsilon_{VG} = 1.40;$$

(2)

$$f'_c = 17 \text{ MPa}, E_f = 110 \text{ GPa}, t_f = 0.650 \text{ mm}, L_f = 100 \text{ mm}, b_f/b_c = 0.25, \varepsilon_{VG} = 1.73;$$

Then, corresponding to the parameter f'_c at 17 MPa, the averaged model factor ε (denoted as ε_{ave}) is calculated as 1.57, i.e., (1.40 + 1.73)/2 = 1.57. The averaged model factor ε_{ave} with respect to different levels of the parameter f'_c could be obtained in this way. By doing a similar procedure for the model factor with respect to all five input parameters, the calculated averaged model factors ε_{ave} are plotted against the specific parameters by hollow dots in Fig. 5. It is shown that ε_{ave} varies nonlinearly with the input parameters. The nonlinear trend with respect to the bond length L_f and FRP width ratio b_f/b_c is quite significant and can be reasonably fitted by a power function and an exponential function with a relative high determination of coefficients (R^2), respectively. For the consistency of the regression equation, the variation of ε_{ave} with three other parameters is also fitted by power or exponential functions. All the core functions for these five parameters are represented as below:

(4a) $$\varepsilon_{ave} \propto E_f^{b_1}$$

(4b) $$\varepsilon_{ave} \propto t_f^{b_2}$$

(4c) $$\varepsilon_{ave} \propto {L_f}^{b_3}$$

(4d) $$\varepsilon_{ave} \propto b_4 \exp(b_f/b_c)$$

(4e) $$\varepsilon_{ave} \propto b_5 \exp(f'_c)$$

where b_i in the above equations is the regression coefficient. Note that in the first step of regression, the specific regression coefficient b_i for each core function is remained to be undetermined. Because each coefficient b_i shown in Eqs. (4a), (4b), (4c), (4d), (4e) represents the general effect coming from the other four parameters.

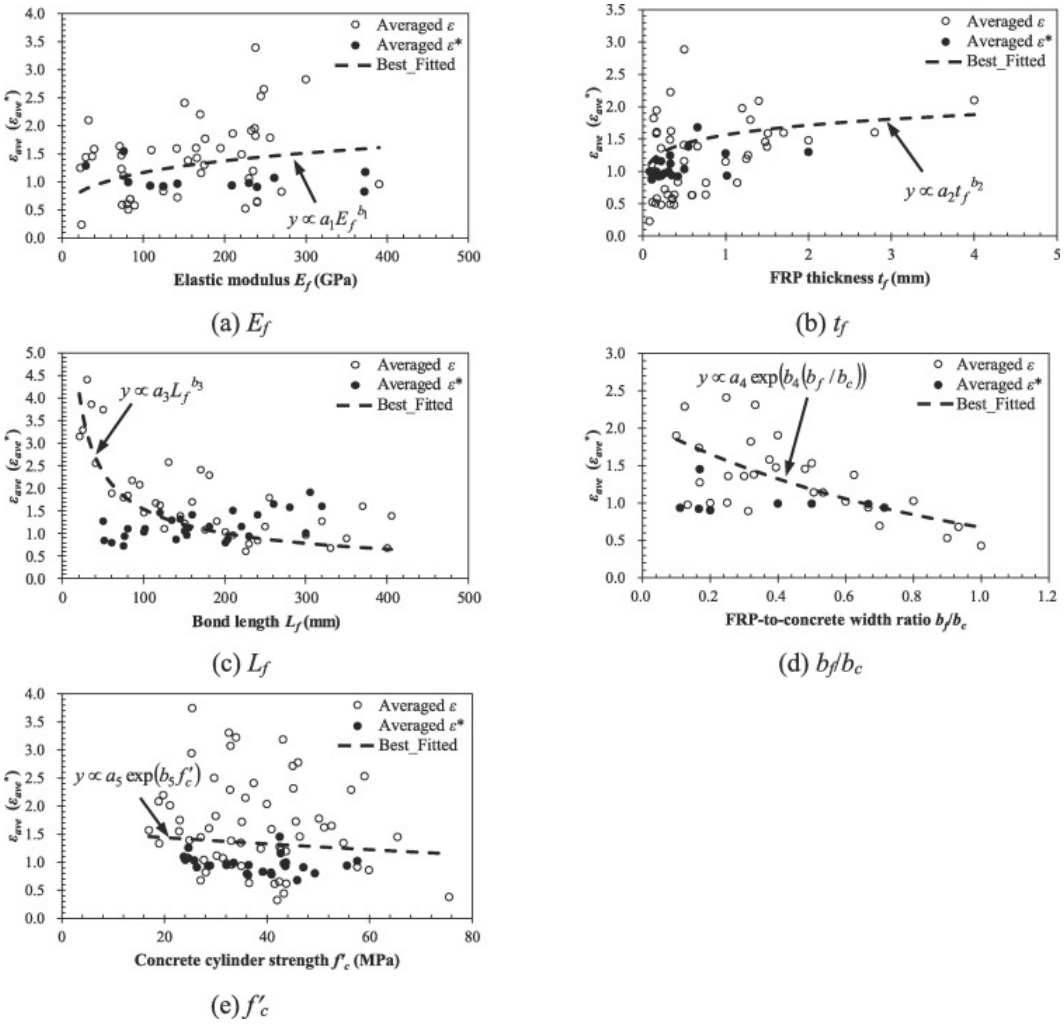

Fig. 5. Variation of averaged model factor ε_{ave} (ε_{ave^*}) with input parameters (void circles for ε from 501 data; solid circles for residual ε^* after removal of dependency, VG Model): (a) FRP elastic modulus E_f, (b) FRP thickness t_f, (c) bond length L_f, (d) FRP-to-concrete width ratio b_f/b_c and (e) concrete cylinder strength f'_c.

The second step is to consider all the core functions together into a general regression equation. Hence, a multiplicative model f can be developed to characterize the systematic variation of ε with the input parameters as follows:

$$f = e^{b_0} \times e^{b_1 \ln E_f} \times e^{b_2 \ln t_f} \times e^{b_3 \ln L_f} \times e^{b_4 (b_f/b_c)} \times e^{b_5 f'_c} \quad (4f)$$

where b_i is the coefficient of the regression equation f. The purpose of the product form of the core functions is that, by conducting a logarithm transformation for both sides of Eq. (4f), the multiplicative form can be changed to a summation form, which is mathematically easy to manage using a multiple linear regression analysis. With the help of the commercial statistic program, SPSS 20, the five regression coefficients b_i were determined as shown in the second column in Table 4. The regression equation f is associated with a high R^2 of 0.88. Then, the model factor for the VG Model can be represented as

(5) $\varepsilon = e^{b_0} \times e^{b_1 \ln E_f} \times e^{b_2 \ln t_f} \times e^{b_3 \ln L_f} \times e^{b_4 (b_f/b_c)} \times e^{b_5 f_c'} \times \varepsilon^*$

where ε^* is the residual of the model factor ε after removing the correlation function f.

Table 4. Coefficients in the regression equation f.

Coefficients	VG Model	HO Model	HW Model	Dai Model
b_0	2.959	0.897	1.343	0.9
b_1	0.395	−0.001	0.003	−0.088
b_2	0.443	0.009	0.452	−0.029
b_3	−0.755	−18.033	−0.001	−17.593
b_4	−0.613	−0.595	−0.621	−0.685
b_5	−0.007	0.001	−10.451	−7.787
R^2	0.882	0.466	0.713	0.466

Apparently, the residual ε^* is a random variable that has no correlation with the five input test parameters for the 501-point-calibration data set because of the regression principles. However, the randomness of ε^*needs to be verified by using another new data set. Hence, the 140-point data set is incorporated here for the verification. The factor ε^* was calculated by using Eq. (5) for each test case. The similar averaging treatment was also adopted for verifying the correlation with the five input parameters. Fig. 5 plots the averaged residual $\varepsilon_{ave}{}^*$ against the parameters as the solid dots. It is graphically validated from Fig. 5 that the nonlinear trend of the model factor for the VG Model has been removed as the $\varepsilon^*{}_{ave}$ distributes randomly along with the line of an averaged $\varepsilon_{ave}{}^*$ equal to 1.00. The third and fifth columns in Table 3show the results of the Spearman correlation analysis in terms of the correlation coefficient R and significance p-value after modification. It is statistically proven that the dependency of the model factor for the VG Model was greatly reduced. Only the FRP thickness t_f is slightly correlated with the residual ε^*, but the correlation was pronouncedly decreased compared to the original model factor ε_{VG}. Hence, it is reasonable to say that the residual ε^* is the random part in the model factor ε_{VG}.

The aforementioned averaging treatment and regression procedure were used to remove the parameter dependency of the model factor for the VG Model. Following a similar approach, the systematic correlation of the model factor for the HO Model, HW Model and Dai Model were removed sequentially. The model factor in Eq. (2) for these models could be represented by Eqs. 6(a) (the HO Model), 6(b) (the HW Model) and 6(c) (the Dai Model) as below:

(6a) $\varepsilon = e^{b_0} \times e^{b_1 E_f} \times e^{b_2 / t_f} \times e^{b_3 / L_f} \times e^{b_4 (b_f/b_c)} \times e^{b_5 f_c'} \times \varepsilon^*$

(6b) $\varepsilon = e^{b_0} \times e^{b_1 E_f} \times e^{b_2 \ln t_f} \times e^{b_3 L_f} \times e^{b_4 (b_f/b_c)} \times e^{b_5 / f_c'} \times \varepsilon^*$

(6c) $\varepsilon = e^{b_0} \times e^{b_1 \ln E_f} \times e^{b_2 t_f} \times e^{b_3 / L_f} \times e^{b_4 (b_f/b_c)} \times e^{b_5 / f_c'} \times \varepsilon^*$

where b_i is the coefficient for regression equation f and ε^* is the random residual of ε that cannot be explained by variation of the design parameters. The residual ε^* can be modeled as a random variable. All the coefficients b_i were determined by the multiple linear regression analysis with the help of SPSS and are shown in Table 4. The determination of coefficient R^2 for those three models is also quite high, e.g., 0.47 for the HO Model, 0.71 for the HW Model and 0.47 for the Dai Model. The detailed modification parameters f for these four modes are given in Appendix I. The histogram of the residual part ε^* of the 501 data points for all the four

regressed model factors, i.e., the VG Model, HO Model, HW Model and Dai Model, are plotted in Fig. 6. The mean values of ε^* for the four models are at about 1.05, which has been moved closer to 1.00 compared with the original mean value of ε shown in Fig. 3. In addition, the mean value is slightly larger than 1.00, which is acceptable since it is considered as conservative for prediction of the ultimate strength. More importantly, the COV values of ε^* for these four models are greatly reduced to an acceptable level of 0.23, i.e., even smaller than the other four good models indicated previously (i.e., the CT Model, *fib* Model, Zhou Model and WJ Model). This is expected because systematic variations have been removed by regression. The modified models can have added value regarding the RBD where COV plays a very important role in the reliability index. So far, the statistics for the random variable of the eight model factors have been fully characterized. Table 5 shows all the statistics for the eight models. All the random model factors follow the lognormal distribution with a mean value ranging from 1.00 to 1.25 and a COV ranging from 0.23 to 0.28. It is reasonable to say that by removing the parameter correlations, the degree of model uncertainties converges to a fairly uniform level.

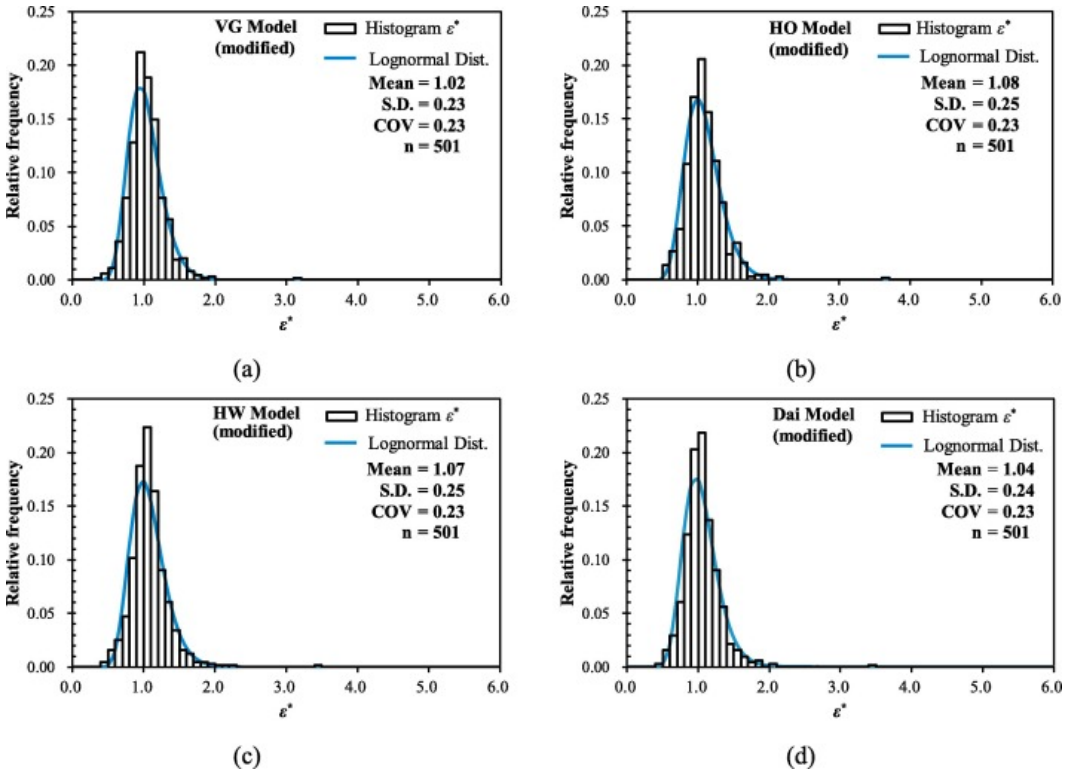

Fig. 6. Histogram of ε^* for 501 data points for the 4 modified models: (a) VG Model, (b) HO Model, (c) HW Model and (d) Dai Model.

Table 5. Statistics of random model factors of the eight models.

Model	Distribution	Mean value	COV	Parameter correlation
CT Model	Lognormal	1.25	0.27	None
fib Model		1.08	0.28	
Zhou Model		1.07	0.27	
WJ Model		1.00	0.27	
VG Model		1.02	0.23	*f* in Eq. (5)
HO Model		1.08	0.23	*f* in Eq. (6a)
HW Model		1.07	0.23	*f* in Eq. (6b)

Model	Distribution	Mean value	COV	Parameter correlation
Dai Model		1.04	0.23	f in Eq. (6c)

When the systematic part f in the original model factor is determined, the calculation model can be modified as

(7a) $$P_u^{c\prime} = f \times P_u^c$$

where $P_u^{c\prime}$ is the modified prediction of the bond strength for the above regressed models. Then, the model factor for these modified calculation models is the residual factor ε^* that is a random variable:

(7b) $$P_u^m = \varepsilon^* \times P_u^{c\prime}$$

Hence, the comparison between the modified prediction $P_u^{c\prime}$ from Eq. (7a) and the test results P_u^m for the four models is re-plotted in Fig. 7. By removing the parameter correlation in the model factor, all the modified predictions are closely distributed around the 45-degree line. Compared to the original data (Fig. 3(e) to (h)), the discrepancy between predicted and experimental results has been noticeably reduced.

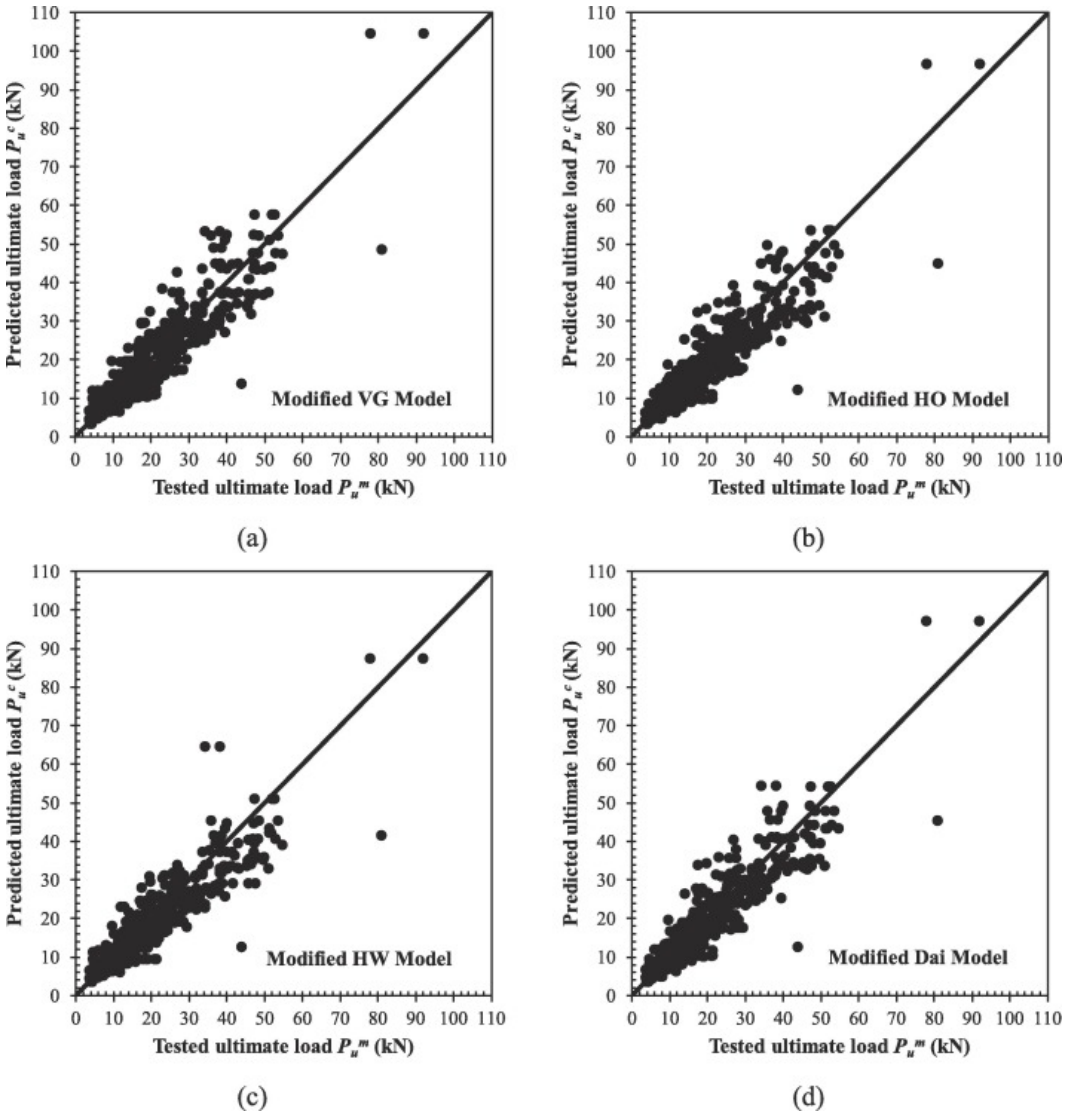

Fig. 7. Comparison between predicted ultimate load and tested ultimate load for the modified four models: (a) VG Model, (b) HW Model, (c) HO Model and (d) Dai Model.

6. Reliability analysis considering model uncertainty

6.1. Limit state function

Similar to the formulation proposed by the ACI code and other literature,[36,37,39] the limit state function for the design of the bond strength for FRP strengthened reinforced concrete is presented as

(8) $$G = R - D - L$$

where G is the limit state function, R is the capacity, and D and L are the demand due to dead load and live load, respectively. The resistance R normally represents the capacity of a structural member such as the flexural capacity of a beam. In FRP retrofitted reinforced concrete beams, however, other parameters such as steel reinforcement also has significant effect on the flexural capacity and it is very hard to single out the reliability of FRP debonding failure in the beam analysis. To clearly investigate the reliability of FRP debonding from concrete substrate, which is the first and key step to understand the reliability of FRP retrofitted reinforced concrete flexural members, the reliability-based design of FRP-to-concrete bonded joints was carried out in this study. Hence, the resistance in this paper is purely referred to the FRP-to-concrete bonded joint resistance without considering the contribution of steel reinforcement in the concrete flexural members. For the design of FRP-to-concrete bonded joints, the resistance R is equal to the test results P_u^m:

(9a) $$R = P_u^m$$

Based on the load and resistance factored design (LRFD),[83] the most commonly used load combination is given as:

(9b) $$S_d = 1.2D_n + 1.6L_n$$

where S_d is the design load, D_n is the nominal dead load, and L_n is the nominal live load. At the design point, the nominal load and resistance are related, and therefore, the nominal dead and live load could be expressed in terms of the resistance[84,85]

(9c) $$S_d = \psi \times P_u^c$$

where ψ is the reduction factor for achieving a reasonable level of the reliability index.[40,86] In the absence of a model factor, the reduction factor is found to be different from model to model ranging from 0.2 to 0.8.[37] However, one major value of this study is to present a calibration of model uncertainties, with which a uniform value of the reduction factor could be obtained. Therefore, a uniform reduction factor ψ was adopted and the magnitude was set as 0.6 to achieve a reasonable reliability index β (around 3.00), based on a trial study on the variation of the reliability index with the reduction factor of the eight models with the modified model factor. Since FRP-to-concrete strengthening may be applied to various loading scenarios, five levels of live-to-dead load ratio $\eta = L_n/D_n$ were selected at 0.50, 0.75, 1.00, 1.25 and 1.50.

6.2. Reliability analysis

For a general reliability analysis, Table 6 includes two commonly used groups of nominal parameters: A and B. The parameters presented here are representative and frequently used in the reliability analysis of FRP-to-concrete bonded joints from literature review. For a specific scenario, the characteristics of each parameter were selected from one of the two groups.[35,87,88,89] Note that the width of FRP b_f and width of concrete b_c are normally separately considered in a design case; therefore, a total of six parameters (i.e., E_f, t_f, L_f, b_f, b_c and f'_c) produced a design space with a sample size of $2^6 = 64$. With consideration of the five levels of live-to-dead load ratio, the total number of reliability analysis cases was about $320 = 2^6 \times 5$. For each case, the first order reliability method (FORM) was adopted to calculate the reliability index β using the Haosofer-Lind approach[90] for the sake of friendly computational effort, compared to the costive Monte Carlo Simulation in terms of run number for a

high reliable case, e.g., $\beta = 5$. The reliability index β can be interpreted geometrically as the distance between the points defined by the expected values of the variables and the closest point on the failure criterion. A general definition of the Haosofer-Lind reliability index β is expressed as below:[91]

$$\beta = \min\sqrt{(x-\mu)^T C^{-1}(x-\mu)} \quad (10)$$

where x is the vector of the uncertain variables in the limit state function, μ is the vector of their means, and C is the covariance matrix for the uncertain variables. By doing a Pearson correlation check of the collected test database, the FRP thickness t_f was found to be related to the FRP modulus E_f with a correlation coefficient ρ at −0.43, as shown in Fig. 8, which is mainly due to the presence of a larger portion of resinwith a low elastic modulus in a thicker FRP. Except t_f and E_f, the other parameters were independent of each other. Basically, the uncertain variables in Eq. (10) need to be normally distributed. For those non-normal variables, e.g., FRP modulus E_f, dead load D and live load L, the Rosenblatt transformation was performed.[92] Details of the transformation procedure can be found in Ang and Tang[41] and are not discussed in detail in this paper.

Table 6. Two nominal groups for the generalized reliability analysis.

Design variables	Probabilistic distribution	Nominal value A	Mean/nominal A	COV A	Nominal value B	Mean/nominal B	COV B	Ref.
FRP thickness t_f	Normal	0.167 (mm)	1.0	0.02	1.2 (mm)	1.0	0.02	Okeil et al. (2013)
FRP modulus E_f	Lognormal	230 (GPa)	1.0	0.12	165 (GPa)	1.0	0.12	Atadero and Karbhari (2008)
Bond length L_f	Deterministic	100 (mm)	–	–	300 (mm)	–	–	–
Bond width b_f	Normal	50 (mm)	1.0	0.02	100 (mm)	1.0	0.02	Okeil et al. (2013)
Concrete width b_c	Normal	150 (mm)	1.01	0.04	200 (mm)	1.01	0.04	Nowak and Szerszen (2003)
Concrete cylinder strength f'_c	Normal	27.56 (MPa)	1.235	0.145	41.3 (MPa)	1.12	0.042	Nowak and Szerszen (2003)
Dead load D	Lognormal	Eq. (9a), (9b), (9c) (kN)	1.05	0.10	Eq. (9a), (9b), (9c) (kN)	1.05	0.10	Galambos et al. (1982)
Live load L	Extreme value I	Eq. (9a), (9b), (9c) (kN)	1.00	0.25	Eq. (9a), (9b), (9c) (kN)	1.00	0.25	Galambos et al. (1982)

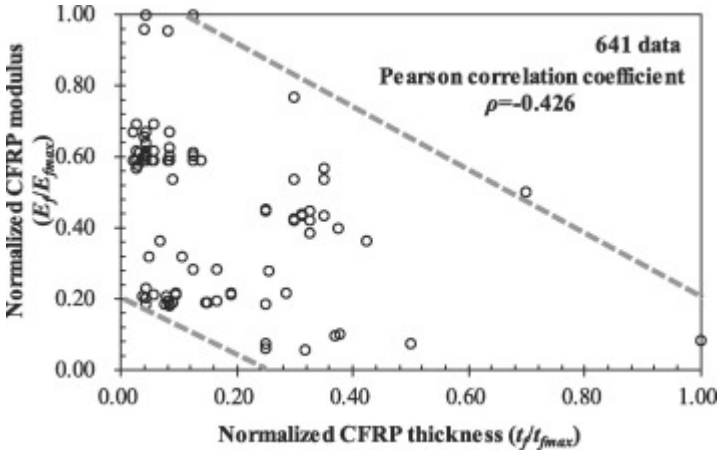

Fig. 8. Correlation of normalized FRP thickness ($t_f/t_{f,max}$) with the normalized FRP modulus ($E_f/E_{f,max}$).

There are a total of three groups of calculated reliability index β, i.e., the first one is for the eight models without the model factor, the second one is with the model factor but the systematic correlation is not removed (unmodified model in short), and the third one is with the model factor where the systematic correlation is removed (modified model in short). It should be specifically noted that the CT Model, *fib*model, Zhou Model and WJ Model are classified into the category of the modified model group in light of the simplicity of description, although they have not been modified since the original COV of these models are small. When given the live-to-dead load ratio η at 1.00, i.e., $D_n = L_n$, Appendix II, Appendix III, Appendix IV list the calculated reliability index β of the 64 design cases based on the eight models. When the model uncertainty is not considered in the analysis, the calculated reliability is the highest among the three groups with an averaged index β at 4.42 as shown in Table 10. Meanwhile, the results of β obtained by the eight models differ from each other significantly, resulting in a high value of COV at about 0.38. When the model uncertainty is considered in the analysis, the calculated β assessed by the unmodified model and modified model is given in Appendix III, Appendix IV, respectively. It is quite clear that the magnitude of the calculated reliability index βdecreases to an average at about 2.70 for the unmodified model and 3.33 for the modified model, respectively. The reliability of design without considering the model uncertainty is quite dangerous where the uncertainty is severely underestimated. By comparing the COV of β for the three groups, the group of modified models has a much smaller magnitude of COV of β at about 0.07 as listed in Appendix IV, compared to the large value at about 0.26 in Appendix III and 0.38 in Appendix II. This result implies that the systematic correlation with design parameters in the model factor ε leads to distinctly different reliability levels for a specific design case. Practically speaking, it is unreasonable that all the design parameters are the same but the output reliability levels are quite different from each other just because of the specific model adopted in the design. This problem has been well addressed by removing the systematic correlation in the model factor εas Appendix IV shows. The merit of the modified model factor should now be appreciated in this sense.

Fig. 9 plots the calculated β against the live-to-dead load ratio η for all 64 design cases. The results of calculated β for models without the model factor, with the unmodified model factor, and with the modified model factor, are illustrated in Fig. 9(a), (b) and (c), respectively. The discrepancy range of the index β in Fig. 9(c) is the narrowest, while the range in Fig. 9(a) is the widest. This again validates that by considering the model factor, the reliability level of the design is much more uniform regardless of the design models. From Fig. 9, the decrease of the calculated index β with the increase of the live-to-dead load ratio η is obvious for models without the model factor, but the trend is not visually observable for models with the model factors (i.e., for both the unmodified model factor and modified model factor). In other words, the effect of ratio η on the reliability of design is limited. This finding is also consistent with the results presented in Wang and Ellingwood.[93]

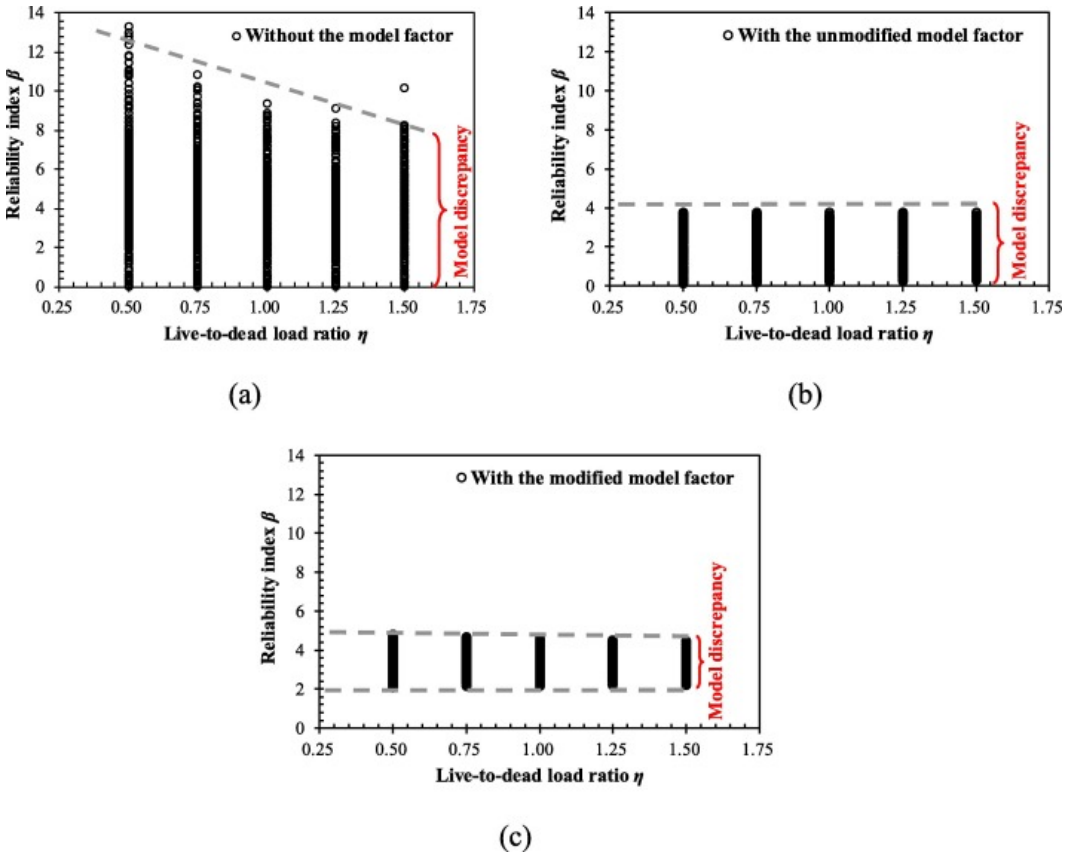

Fig. 9. Reliability analysis for 64 cases under different live-to-dead load ratio η: (a) without the model factor, (b) with the unmodified model factor and (c) with the modified model factor.

6.3. Reliability-based joint design

Compared to the reliability analysis, the reliability-based design is a backward procedure where the nominal or mean values of the design parameters are to be determined to achieve the required reliability index $\beta_{required}$. Fig. 10 describes a design flow considering uncertainties in parameters, models and loads. The limit state function G, as shown in Fig. 10, is similar to the function proposed in Eq. (8). For the design without the model factor, the ε in the limit function G in Fig. 10 is constantly equal to 1.00. For the design with the unmodified model factor, the ε is arbitrarily "seen" as a lognormal random variable with the statistics shown in Fig. 3. For the design with the modified model factor, the ε is consisted of the systematic part f and the residual random part ε^* that is described by the random variable summarized in Table 5. Again, the Haosofer-Lind (FORM) reliability method is adopted to calculate the reliability index β for the trial design point. The iterative loop is necessary until the calculated index β for the trial design point is not less than the required magnitude $\beta_{required}$. For the probability-based limit state design of structures, $\beta_{required}$ at about 3.00 is frequently used in designs and in the literature.[89,94] Among all the parameters of FRP-to-concrete bonded joints, the FRP thickness t_f and bond width $b_f$are the common parameters to be determined for a retrofitting case. Hence, following two examples will be discussed in detail. The first example was based on a one-parameter design where b_f was the only parameter to be determined. The second example was based on a two-parameter design where both t_f and b_f were the parameters to be determined. It should also be pointed out that only CFRP sheets were used in the present analysis for the sake of simplicity.

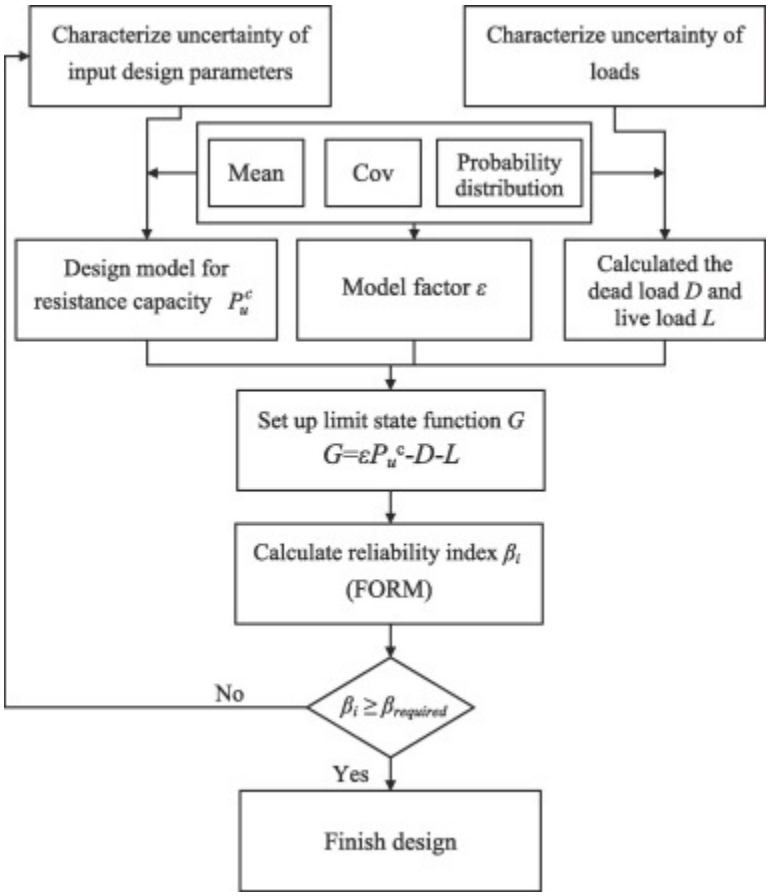

Fig. 10. Design flowchart of the RBD considering the model factor.

6.3.1. One-parameter design

For the one-parameter design, the statistics in terms of mean value, COV and probability distribution type for the five input parameters, E_f, t_f, L_f, b_c and f'_c, were all known to designers as shown in Table 7. Only the mean value of CFRP width b_f was unknown and to be determined; however, the COV and distribution type of b_f were also known as given in Table 7. The dead load D was prescribed as a lognormal random variable with a mean value at 6 kN and a COV of 0.1, while the live load L was set to be an extreme value type I random variable with a mean value at 3 kN and a COV at 0.25. The optimization procedure for finding the best b_f presented by the design flowchart in Fig. 10 was treated simply by the grid method. Since the width of concrete was set at 150 mm, the potential design points for the width of CFRP b_f were selected with an incremental step of 2 mm ranging from 10 to 150 mm, i.e., b_f = 10 mm, 12 mm, 14 mm, …, 150 mm. The calculated design points of width b_f for the three groups are shown in Table 8. The results in the second row are from the models without the model factor. The results in the third row are from models with the unmodified model factor, and the results in the fourth row are from models with the modified model factor. Comparatively speaking, the magnitude of the design width b_f without the model factor is smallest among the results for the three groups, i.e., ranging from 24 to 76 mm. This is in conformance with the findings in reliability analysis conducted in the previous section where the reliability was severely overestimated when the model factor was not considered, as shown in Appendix II. For the design with the unmodified model factor, the designed width b_f ranges from 42 to 110 mm. It is much larger than the design without the model factor, which is to be expected based on the comparison shown between Appendix II, Appendix III. Similar to the design without the model factor, the discrepancy of the calculated width b_f by different models with the unmodified model factor is still notably high. For the design with the modified model factor, the design range of b_f is from 40 to 46 mm, which is much narrower and more reasonable compared to the results from the design without the model factor and with the

unmodified model factor. Thus, the uniform design for all eight models given by the calibrated model factors is well validated by the one-parameter reliability-based design case.

Table 7. Statistics for reliability based design.

Parameter		Mean	COV	Distribution	Correlation
Pre-determined parameters	CFRP modulus E_f(GPa)	248.3	0.12	Lognormal	$\rho E_f,\ t_f = -0.43$
	CFRP length L_f (mm)	250	0	Determined	/
	Concrete width b_c(mm)	150	0.04	Normal	/
	Concrete cylinder strength f'_c (MPa)	32.92	0.145	Normal	/
	Dead load D (kN)	6.0	0.1	Lognormal	/
	Live load L (kN)	3.0	0.25	Extreme value I	/
One-parameter design	CFRP thickness t_f(mm)	0.501	0.02	Normal	$\rho E_f,\ t_f = -0.43$
	CFRP width b_f (mm)	X_1	0.02	Normal	/
Two-parameter design	CFRP thickness t_f(mm)	X_2	0.02	Normal	$\rho E_f,\ t_f = -0.43$
	CFRP width b_f (mm)	X_3	0.02	Normal	/

Table 8. Design results of width of CFRP for eight models.

	Width of CFRP b_f (mm)							
	VG Model	**HO Model**	**HW Model**	**CT Model**	***fib*Model**	**Dai Model**	**Zhou Model**	**WJ Model**
W/o model factor	42	48	76	31	29	25	26	24
Unmodified factor	110	60	90	44	46	60	42	42
Modified factor	40	42	40	42	46	40	42	42

6.3.2. Two-parameter design

For the two-parameter reliability-based design, as shown in Table 7, the statistics of the four parameters, E_f, L_f, b_c and f'_c, were pre-determined by the mean value, COV, and the distribution types were the same as those in the one-parameter design. The mean values of FRP thickness t_f and width b_f, were unknown design parameters whereas COVs for $t_f$and b_f were known, as shown in Table 7. To obtain the optimized pair of design points (t_f, b_f), the simple grid method was used. The design points of b_f were selected every 5 mm from 30 to 120 mm, while the $t_f$was selected every 0.167 mm (the thickness of one layer of CFRP) from 0.167 (1 layer) to 1.67 mm (10 layers). Hence, there was a grid mesh (b_f, t_f) for the size of 19 × 10 with a total of 190 design points. By doing the reliability analysis of the 190 design points, a calculated reliability index β surface was identified and is plotted in Fig. 11, which presents the modified Dai Model as an example. The red dots in Fig. 11are the specific β for each design point. For simplicity, the CFRP thickness t_f is represented by the number of layers. The required magnitude of β is also plotted as the blue surface constantly located at the level of β equal to 3.00. The calculated β surface, intersects with the required β surface and the intersected red line in Fig. 11 is the design curve for the two-parameter designs.

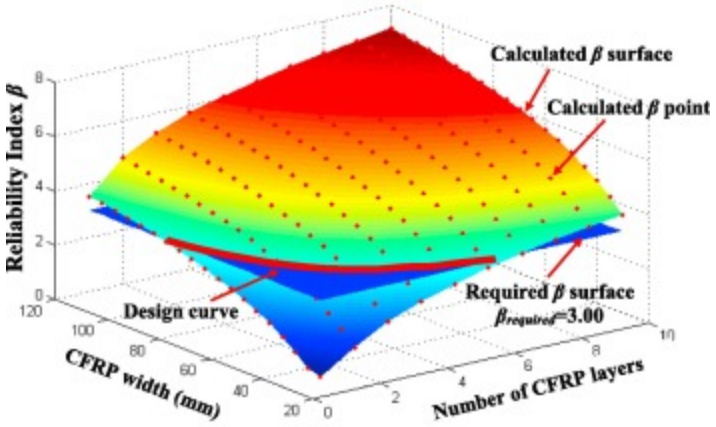

Fig. 11. Design curve in the two-parameter-design space (Dai Model).

Fig. 12 uses plan view mapping to illustrate charts of different design curves under specific design requirements ($\beta_{required}$) with the modified model factor. It is clear from Fig. 12 that contour lines of different reliability levels are comparable for all eight models from Fig. 12(a) to (h). On the contrary, Fig. 13, Fig. 14 have similar contour lines for design with the unmodified model factor and without the model factor, respectively. It is evident that the design curves for the two design groups are significantly different in terms of magnitude and distribution of calculated β. Furthermore, for the HW Model and VG Model, the design curves of β are independent of the FRP thickness, which are greatly different from the curves for other models. The merit of the modified model factor in the reliability-based design is, thus, verified by the two-parameter design case.

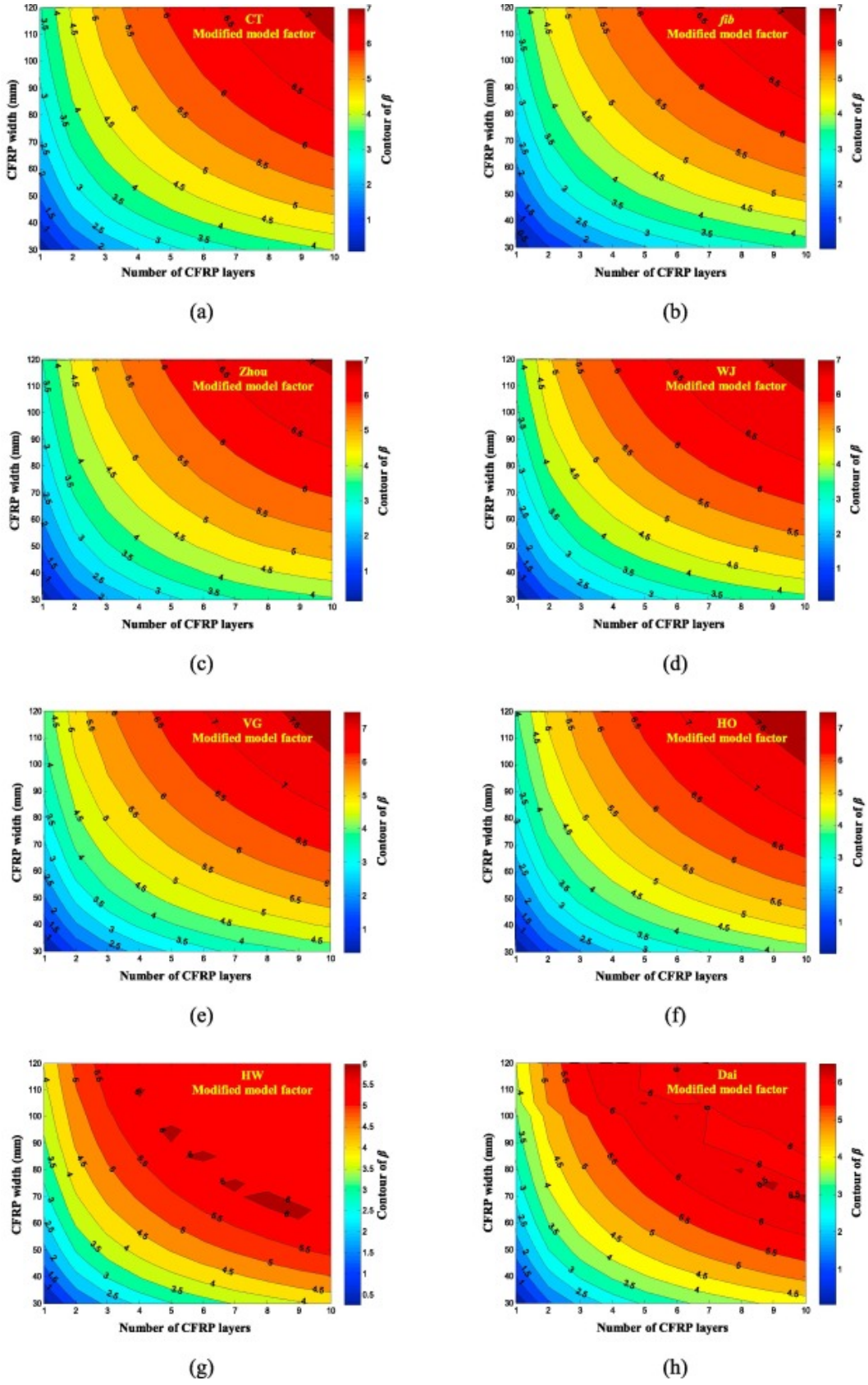

Fig. 12. Design chart for the two-parameter design with modified model factors: (a) CT Model, (b) *fib* Model, (c) Zhou Model, (d) WJ Model, (e) VG Model, (f) HO Model, (g) HW Model and (h) Dai Model.

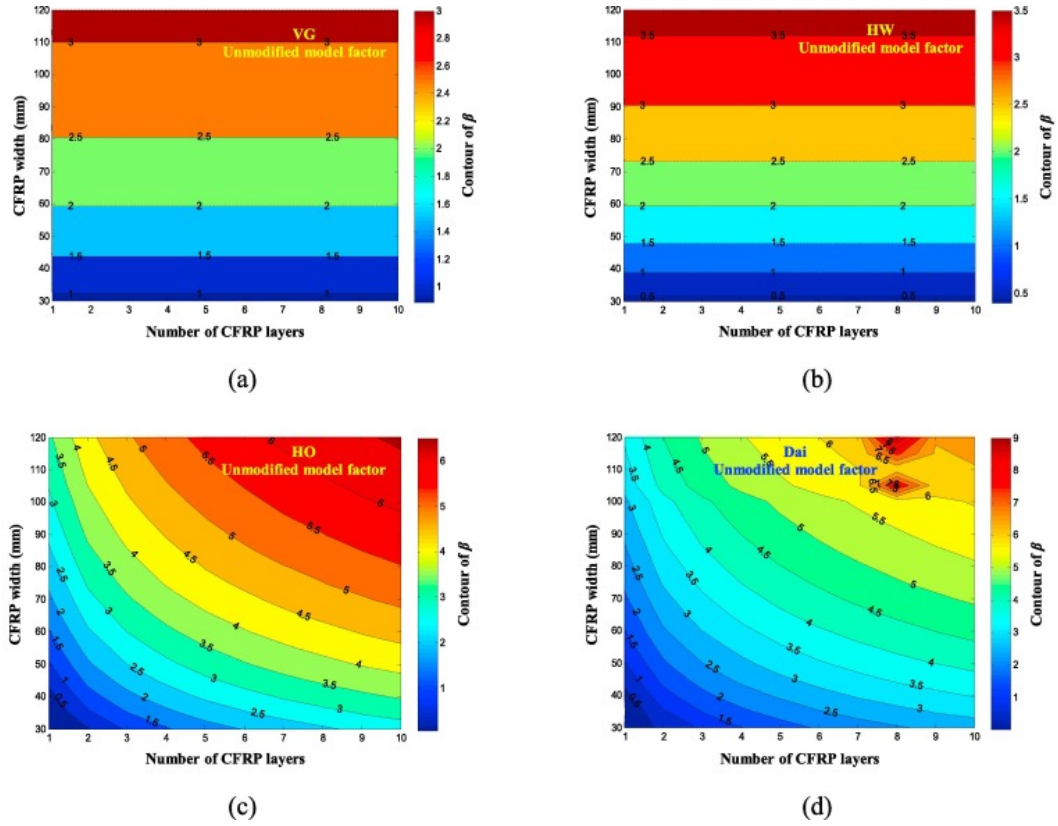

Fig. 13. Design chart for the two-parameter design with the unmodified model factors: (a) VG Model, (b) HO Model, (c) HW Model and (d) Dai Model.

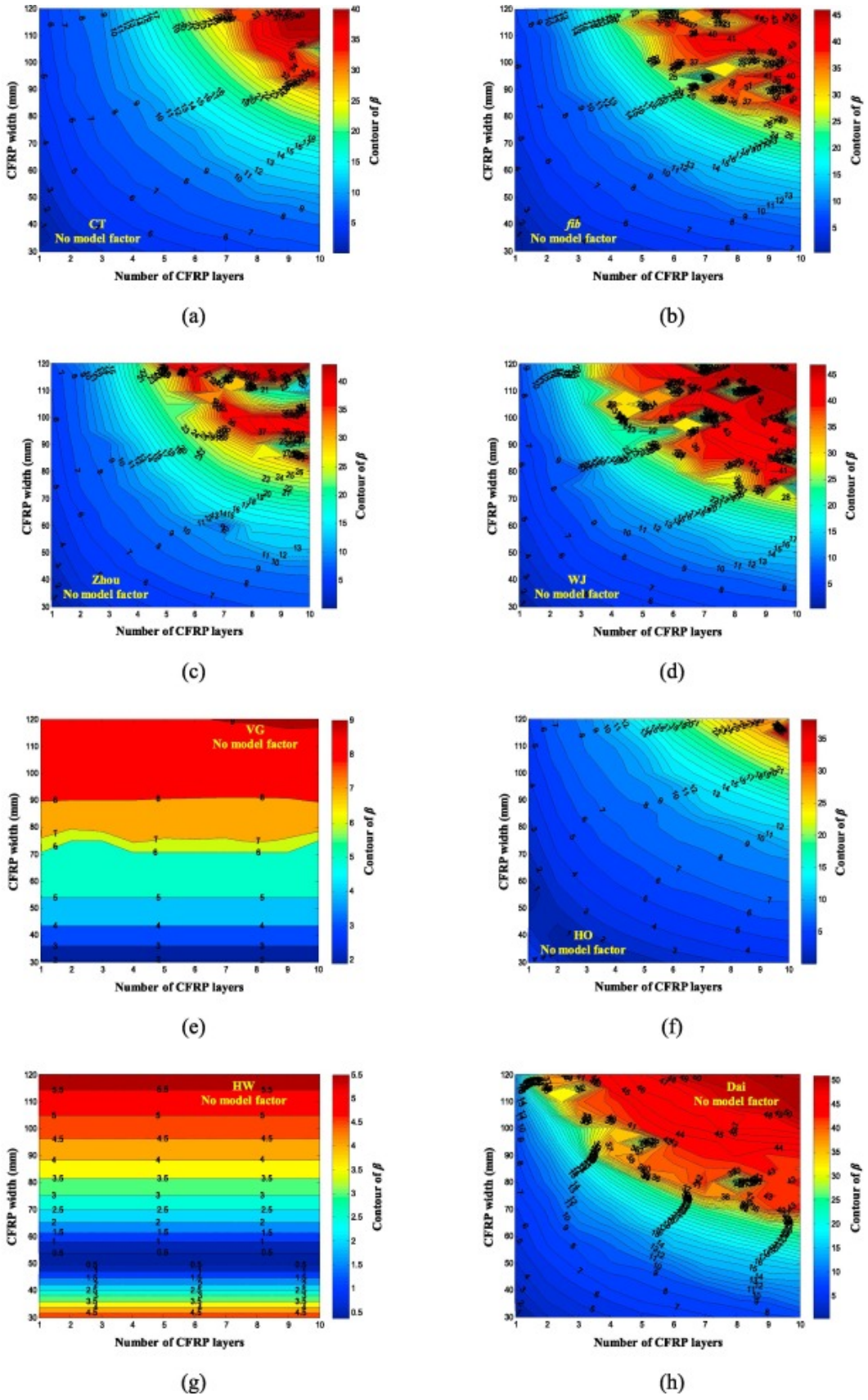

Fig. 14. Design chart for the two-parameter design without considering the model factor: (a) CT Model, (b) *fib* Model, (c) Zhou Model, (d) WJ Model, (e) VG Model, (f) HO Model, (g) HW Model and (h) Dai Model.

7. Conclusions

This paper presents a framework for a full probabilistic analysis of FRP-to-concrete bonded joints considering the uncertainties of prediction models in a manner. Eight frequently used prediction models were adopted; namely the Van Gemert (VG) (1980) model, the Holzenkämpfer (HO) (1994) model, the Hiroyuki and Wu (HW) (1997) model, the Chen and Teng (CT) (2001) model, the *fib* (2001) model, the Dai et al. (Dai) (2005) model, the Zhou (2009) model and the Wu and Jiang (WJ) (2013) model. The model uncertainty was quantitatively evaluated by a model factor ε which was defined as the ratio of the measured bond strength from the test results to the predicted value. In total, 641 shear pull-out test cases were extensively collected to calibrate the model factor. The model factor ε should only represent the predictability of a model and, thus, should be a random variable regardless of input parameters. However, after checking the randomness of the model factors, four of the eight models (i.e., the VG Model, HO Model, HW Model and Dai Model) were found to have a model factor that was correlated with the input parameters. The other four models (i.e., CT Model, *fib* Model, Zhou Model and WJ Model) have a random model factor that is lognormally distributed with a mean value ranging from 1.00 to 1.25 and a COV ranging from 0.27 to 0.28.

For those four models with the model factor depending on the input parameters, 501 cases in the database were used to remove the systematical part of the model factor ε by using a newly built multiple regression equation f in this study. The randomness of residual factor ε^* after regression was well verified by the remaining 140 cases in the database. By doing the detailed calibration, the characterized model factors of the four models became lognormally distributed random variables with a mean value ranging from 1.02 to 1.08, and a COV at 0.23. Note that the original model factors without removing systematic correlations had mean values ranging from 0.86 to 2.24 and COV ranging from 0.27 to 0.66. The calibration, thus, greatly improved both the accuracy and precision of the prediction models. Furthermore, the application examples clearly indicated the merit of considering model uncertainties in the reliability analysis that could automatically reduce the variation of joint design to a fairly uniform level. To be more specific, the required reliability level of a joint design case is achieved to be at the same level (i.e., β is constant at 3.00 in this paper) by a similar set of design parameters regardless of the specific model used.

This study extends the understanding of the performance of FRP-to-concrete bond strength prediction models. Based on the approach presented in this study, the model uncertainties of different prediction models converge to a uniform level. This knowledge should be of great help for determining the appropriate reduction factor ψ in the reliability analysis since the factors ψ are different for prediction models with various model uncertainties. It is also desirable for design codes and guidelines to standardize the calibration of model uncertainties and to involve the existing prediction models for the strengthening method.

Acknowledgements

The work described in this paper was supported by the National Natural Science Foundation of China (NSFC Grant Nos. 51508406 and 51608380). The authors are grateful for these programs. The authors also wish to express their heartfelt appreciation to Prof. Kok-Kwang Phoon from National University of Singapore for supervising the work.

Appendixes

Appendix I. Modification parameters f for VG, HO, HW and Dai Models.

VG Model	$f = e^{2.959} \times e^{0.395\ln E_f} \times e^{0.443\ln t_f} \times e^{-0.755\ln L_f}$

$$\times e^{-0.613\left(\frac{b_f}{b_c}\right)} \times e^{-0.007 f_c'}$$

HO Model

$$f = e^{0.897} \times e^{-0.001 E_f} \times e^{0.009/t_f} \times e^{-\frac{18.033}{L_f}} \times e^{-0.595\left(\frac{b_f}{b_c}\right)} \times e^{0.001 f_c'}$$

HW Model

$$f = e^{1.343} \times e^{0.003 E_f} \times e^{0.452 \ln t_f} \times e^{-0.001 L_f} \times e^{-0.621\left(\frac{b_f}{b_c}\right)} \times e^{-10.451/f_c'}$$

Dai Model

$$f = e^{0.9} \times e^{-0.088 \ln E_f} \times e^{-0.029 t_f} \times e^{-\frac{17.593}{L_f}} \times e^{-0.685\left(\frac{b_f}{b_c}\right)} \times e^{-7.787/f_c'}$$

Appendix II. Reliability index of 64 cases without considering the model factor.

Case No.	VG-β	HO-β	HW-β	CT-β	Fib-β	Dai-β	Zhou-β	WJ-β	COV of β
1	2.89	2.95	2	4.64	5.22	6.01	5.34	5.71	0.35
2	3.6	3.06	1.58	4.72	5.37	5.86	5.43	5.74	0.35
3	2.78	2.84	1.87	4.79	5.12	5.9	5.52	5.78	0.37
4	3.49	2.95	1.43	4.87	5.26	5.75	5.61	5.82	0.36
5	3.32	3.4	2.51	4.07	4.92	6.65	4.77	5.35	0.3
6	4.06	3.52	2.13	4.15	5.07	6.59	4.86	5.31	0.3
7	3.1	3.17	2.25	4.35	4.96	6.36	5.02	5.55	0.32
8	3.82	3.29	1.85	4.43	5.11	6.08	5.12	5.54	0.31

Case No.	VG-β	HO-β	HW-β	CT-β	Fib-β	Dai-β	Zhou-β	WJ-β	COV of β
9	6.92	1.99	2.9	3.77	4.36	5.12	4.47	4.9	0.35
10	8.08	2.03	2.47	3.79	4.43	4.91	4.5	4.84	0.42
11	6.98	1.89	2.81	3.94	4.28	5.04	4.67	4.98	0.35
12	7.9	1.93	2.37	3.96	4.35	4.82	4.69	4.93	0.42
13	6.4	2.39	3.28	3.1	3.97	5.47	3.81	4.52	0.32
14	8.49	2.43	2.86	3.11	4.04	5.26	3.83	4.39	0.45
15	6.36	2.19	3.08	3.43	4.06	5.29	4.12	4.72	0.32
16	8.25	2.23	2.66	3.45	4.13	5.08	4.14	4.63	0.43
17	3.5	2.81	2.72	4.51	5.09	5.87	5.2	5.61	0.28
18	4.24	2.91	2.34	4.58	5.23	5.71	5.29	5.62	0.28
19	3.4	2.7	2.61	4.66	4.99	5.77	5.38	5.68	0.3
20	4.13	2.8	2.22	4.74	5.12	5.61	5.48	5.7	0.3
21	3.9	3.24	3.18	3.92	4.77	6.5	4.61	5.27	0.25
22	4.68	3.36	2.82	3.99	4.91	6.39	4.7	5.22	0.25
23	3.69	3.02	2.94	4.2	4.82	6.08	4.88	5.45	0.26
24	4.45	3.13	2.58	4.28	4.96	5.92	4.97	5.44	0.25
25	7.73	1.7	3.46	3.53	4.12	4.88	4.23	4.66	0.4
26	8.75	1.73	3.03	3.53	4.18	4.66	4.24	4.58	0.47
27	7.65	1.61	3.37	3.71	4.04	4.8	4.43	4.74	0.4
28	8.61	1.63	2.94	3.71	4.1	4.57	4.44	4.68	0.46
29	6.5	2.09	3.8	2.82	3.71	5.21	3.55	4.26	0.34
30	9.37	2.12	3.38	2.82	3.77	4.99	3.55	4.12	0.52
31	6.47	1.89	3.62	3.18	3.81	5.04	3.87	4.47	0.33
32	8.92	1.92	3.2	3.17	3.86	4.82	3.87	4.36	0.49
33	0.79	4.53	2.97	4.3	5.27	8.04	4.74	5.4	0.46
34	0.38	4.53	3.88	4.72	5.8	7.76	5.33	5.58	0.44
35	0.97	4.42	3.2	4.44	5.16	7.92	4.9	5.57	0.43
36	0.59	4.41	4.11	4.86	5.67	7.62	5.5	5.79	0.42
37	0.11	4.97	2.08	3.75	4.99	8.7	4.21	4.51	0.59
38	0.43	5.01	2.94	4.16	5.53	8.24	4.77	4.56	0.5
39	0.48	4.73	2.56	4.01	5.01	8.25	4.44	4.98	0.52
40	0.01	4.76	3.45	4.42	5.54	8.03	5.01	5.1	0.5
41	3.49	3.06	2.61	4.74	5.32	6.11	5.43	5.84	0.29

Case No.	VG-β	HO-β	HW-β	CT-β	Fib-β	Dai-β	Zhou-β	WJ-β	COV of β
42	4.22	3.15	3.31	4.81	5.45	5.94	5.52	5.84	0.23
43	3.39	2.94	2.83	4.89	5.21	6	5.61	5.9	0.29
44	4.11	3.03	3.52	4.96	5.34	5.83	5.7	5.92	0.23
45	3.91	3.5	1.74	4.17	5.02	6.82	4.87	5.51	0.34
46	4.68	3.61	2.42	4.24	5.16	6.58	4.95	5.45	0.27
47	3.69	3.27	2.19	4.45	5.06	6.45	5.12	5.69	0.31
48	4.44	3.37	2.88	4.52	5.19	6.16	5.2	5.66	0.24
49	0.21	4.17	2.21	4.53	5.4	7.57	4.93	5.61	0.52
50	0.29	4.17	3.12	4.92	5.88	7.26	5.48	5.76	0.46
51	0.38	4.05	2.44	4.66	5.29	7.42	5.08	5.76	0.49
52	0.09	4.04	3.36	5.06	5.75	7.17	5.65	5.93	0.47
53	0.47	4.62	1.28	4	5.14	8.1	4.42	4.81	0.58
54	1.05	4.66	2.13	4.38	5.62	7.81	4.94	4.84	0.47
55	0.11	4.38	1.77	4.25	5.16	7.75	4.64	5.23	0.56
56	0.66	4.4	2.65	4.63	5.63	7.5	5.17	5.33	0.46
57	4.1	2.93	1.34	4.62	5.2	5.99	5.32	5.74	0.36
58	4.87	3.02	2.05	4.68	5.33	5.81	5.39	5.73	0.3
59	4	2.82	1.55	4.77	5.1	5.88	5.5	5.8	0.35
60	4.76	2.91	2.26	4.83	5.22	5.71	5.57	5.81	0.29
61	4.49	3.37	0.54	4.04	4.89	6.58	4.74	5.42	0.42
62	5.32	3.47	1.19	4.1	5.02	6.45	4.81	5.35	0.36
63	4.28	3.14	0.95	4.32	4.94	6.2	5	5.59	0.38
64	5.09	3.24	1.63	4.39	5.06	6.03	5.07	5.55	0.32
Average	*4.42*								***0.38***

Appendix III. Reliability index of 64 cases with the unmodified model factor considered.

Case No.	VG-β	HO-β	HW-β	CT-β	Fib-β	Dai-β	Zhou-β	WJ-β	COV of β
1	1.3	2.6	2.36	3.45	3.29	2.59	3.45	3.47	0.27
2	1.47	2.64	2.19	3.48	3.35	2.49	3.48	3.46	0.27
3	1.27	2.53	2.31	3.55	3.22	2.53	3.57	3.52	0.29
4	1.43	2.58	2.14	3.58	3.28	2.43	3.6	3.52	0.28
5	1.46	2.85	2.58	3.06	3.09	2.84	3.06	3.21	0.2
6	1.63	2.9	2.42	3.1	3.15	2.75	3.09	3.17	0.19
7	1.38	2.72	2.47	3.25	3.11	2.71	3.23	3.35	0.23

Case No.	VG-β	HO-β	HW-β	CT-β	Fib-β	Dai-β	Zhou-β	WJ-β	COV of β
8	1.54	2.77	2.3	3.29	3.17	2.62	3.27	3.33	0.22
9	2.76	2.08	2.76	2.86	2.71	2.08	2.85	2.92	0.13
10	2.92	2.08	2.56	2.85	2.72	1.95	2.84	2.86	0.15
11	2.73	2.02	2.71	2.97	2.65	2.03	2.99	2.98	0.15
12	2.89	2.03	2.52	2.96	2.66	1.9	2.98	2.93	0.16
13	2.88	2.28	2.93	2.4	2.44	2.28	2.39	2.66	0.1
14	3.04	2.29	2.74	2.39	2.46	2.15	2.38	2.56	0.11
15	2.82	2.17	2.84	2.62	2.5	2.18	2.61	2.8	0.1
16	2.98	2.19	2.65	2.61	2.51	2.05	2.6	2.72	0.12
17	1.52	2.51	2.67	3.36	3.2	2.51	3.36	3.41	0.23
18	1.69	2.56	2.5	3.39	3.26	2.41	3.39	3.39	0.22
19	1.49	2.45	2.62	3.46	3.13	2.45	3.48	3.45	0.25
20	1.65	2.5	2.45	3.49	3.19	2.35	3.51	3.45	0.24
21	1.67	2.76	2.88	2.95	2.98	2.75	2.95	3.16	0.17
22	1.84	2.81	2.72	2.99	3.04	2.66	2.99	3.12	0.15
23	1.59	2.63	2.77	3.15	3.02	2.63	3.13	3.29	0.19
24	1.76	2.68	2.61	3.18	3.07	2.53	3.17	3.26	0.18
25	2.94	1.93	3.01	2.69	2.54	1.94	2.68	2.76	0.16
26	3.1	1.93	2.81	2.67	2.55	1.8	2.67	2.69	0.17
27	2.91	1.88	2.97	2.81	2.49	1.89	2.82	2.81	0.17
28	3.07	1.88	2.77	2.79	2.49	1.75	2.81	2.75	0.19
29	3.06	2.12	3.18	2.21	2.26	2.13	2.21	2.47	0.17
30	3.21	2.13	2.98	2.19	2.27	1.99	2.19	2.36	0.18
31	3	2.02	3.09	2.45	2.33	2.03	2.43	2.62	0.16
32	3.15	2.03	2.89	2.43	2.33	1.89	2.41	2.54	0.17
33	0.27	3.52	0.89	3.24	3.37	3.5	3.11	3.25	0.49
34	0.38	3.49	0.65	3.43	3.57	3.33	3.35	3.3	0.5
35	0.23	3.45	0.83	3.34	3.3	3.44	3.22	3.37	0.5
36	0.34	3.42	0.59	3.52	3.48	3.26	3.46	3.43	0.51
37	0.43	3.78	1.11	2.86	3.18	3.76	2.73	2.62	0.47
38	0.55	3.77	0.9	3.06	3.39	3.61	2.98	2.62	0.47
39	0.34	3.64	0.99	3.04	3.19	3.62	2.89	2.95	0.48
40	0.46	3.62	0.77	3.24	3.4	3.46	3.14	2.98	0.48

Case No.	VG-β	HO-β	HW-β	CT-β	Fib-β	Dai-β	Zhou-β	WJ-β	COV of β
41	1.52	2.65	0.98	3.52	3.36	2.65	3.51	3.56	0.36
42	1.68	2.69	0.8	3.54	3.4	2.54	3.54	3.54	0.38
43	1.48	2.59	0.92	3.62	3.28	2.58	3.63	3.6	0.38
44	1.64	2.62	0.75	3.64	3.33	2.48	3.65	3.59	0.39
45	1.67	2.91	1.2	3.13	3.16	2.9	3.13	3.32	0.29
46	1.84	2.95	1.03	3.16	3.21	2.8	3.15	3.27	0.3
47	1.59	2.78	1.09	3.32	3.18	2.77	3.3	3.45	0.33
48	1.76	2.82	0.91	3.34	3.23	2.67	3.33	3.41	0.34
49	0.41	3.3	1.08	3.4	3.45	3.29	3.23	3.38	0.45
50	0.52	3.28	0.85	3.56	3.62	3.12	3.45	3.42	0.47
51	0.37	3.23	1.02	3.49	3.38	3.22	3.34	3.49	0.46
52	0.48	3.21	0.79	3.66	3.54	3.05	3.56	3.53	0.48
53	0.57	3.57	1.32	3.03	3.27	3.55	2.86	2.82	0.42
54	0.7	3.57	1.1	3.21	3.46	3.41	3.1	2.81	0.42
55	0.48	3.43	1.19	3.2	3.28	3.41	3.02	3.12	0.43
56	0.61	3.42	0.97	3.38	3.46	3.26	3.25	3.14	0.44
57	1.74	2.58	1.3	3.44	3.28	2.58	3.43	3.5	0.31
58	1.91	2.61	1.12	3.46	3.32	2.47	3.45	3.47	0.32
59	1.71	2.52	1.25	3.54	3.21	2.52	3.55	3.54	0.33
60	1.87	2.55	1.07	3.56	3.25	2.41	3.57	3.52	0.34
61	1.89	2.83	1.52	3.04	3.07	2.82	3.04	3.27	0.23
62	2.06	2.87	1.34	3.06	3.11	2.72	3.06	3.21	0.24
63	1.82	2.7	1.41	3.23	3.1	2.7	3.22	3.39	0.27
64	1.98	2.74	1.23	3.25	3.14	2.59	3.24	3.35	0.28
Average	***2.70***								***0.28***

Appendix IV. Reliability index of 64 cases with the modified model factor considered.

Case No.	VG-β	HO-β	HW-β	CT-β	Fib-β	Dai-β	WJ-β	Zhou-β	COV of β
1	3.27	3.42	3.33	3.45	3.29	3.42	3.47	3.45	0.02
2	3.35	3.54	3.4	3.48	3.35	3.55	3.46	3.48	0.02
3	3.36	3.51	3.42	3.55	3.22	3.53	3.52	3.57	0.03
4	3.44	3.62	3.49	3.58	3.28	3.66	3.52	3.6	0.04
5	2.91	3.07	2.96	3.06	3.09	2.97	3.21	3.06	0.03

Case No.	VG-β	HO-β	HW-β	CT-β	Fib-β	Dai-β	WJ-β	Zhou-β	COV of β
6	2.99	3.2	3.03	3.1	3.15	3.11	3.17	3.09	0.02
7	3.08	3.24	3.14	3.25	3.11	3.19	3.35	3.23	0.03
8	3.16	3.36	3.21	3.29	3.17	3.32	3.33	3.27	0.02
9	3.53	3.18	3.24	2.86	2.71	3.16	2.92	2.85	0.09
10	3.57	3.25	3.26	2.85	2.72	3.25	2.86	2.84	0.1
11	3.64	3.28	3.34	2.97	2.65	3.29	2.98	2.99	0.1
12	3.68	3.35	3.37	2.96	2.66	3.38	2.93	2.98	0.1
13	3.1	2.76	2.8	2.4	2.44	2.65	2.66	2.39	0.09
14	3.14	2.83	2.82	2.39	2.46	2.74	2.56	2.38	0.1
15	3.31	2.97	3.02	2.62	2.5	2.9	2.8	2.61	0.09
16	3.35	3.04	3.04	2.61	2.51	2.99	2.72	2.6	0.1
17	3.29	3.53	3.19	3.36	3.2	3.41	3.41	3.36	0.03
18	3.36	3.64	3.25	3.39	3.26	3.54	3.39	3.39	0.04
19	3.38	3.62	3.28	3.46	3.13	3.53	3.45	3.48	0.04
20	3.46	3.73	3.35	3.49	3.19	3.66	3.45	3.51	0.05
21	2.91	3.17	2.8	2.95	2.98	2.95	3.16	2.95	0.04
22	2.99	3.29	2.87	2.99	3.04	3.09	3.12	2.99	0.04
23	3.09	3.34	2.99	3.15	3.02	3.18	3.29	3.13	0.04
24	3.17	3.46	3.06	3.18	3.07	3.31	3.26	3.17	0.04
25	3.47	3.2	3.01	2.69	2.54	3.08	2.76	2.68	0.11
26	3.5	3.27	3.03	2.67	2.55	3.16	2.69	2.67	0.12
27	3.58	3.31	3.13	2.81	2.49	3.21	2.81	2.82	0.12
28	3.61	3.38	3.14	2.79	2.49	3.3	2.75	2.81	0.13
29	3.03	2.78	2.55	2.21	2.26	2.55	2.47	2.21	0.12
30	3.05	2.84	2.57	2.19	2.27	2.63	2.36	2.19	0.13
31	3.24	2.99	2.78	2.45	2.33	2.81	2.62	2.43	0.12
32	3.27	3.06	2.8	2.43	2.33	2.89	2.54	2.41	0.13
33	4.05	4.41	4.15	3.24	3.37	4.45	3.25	3.11	0.15
34	4.04	4.44	4.13	3.43	3.57	4.5	3.3	3.35	0.13
35	4.13	4.49	4.23	3.34	3.3	4.55	3.37	3.22	0.15
36	4.12	4.52	4.21	3.52	3.48	4.6	3.43	3.46	0.13
37	3.7	4.09	3.8	2.86	3.18	4.03	2.62	2.73	0.18
38	3.71	4.14	3.8	3.06	3.39	4.1	2.62	2.98	0.16

Case No.	VG-β	HO-β	HW-β	CT-β	Fib-β	Dai-β	WJ-β	Zhou-β	COV of β
39	3.86	4.24	3.96	3.04	3.19	4.23	2.95	2.89	0.16
40	3.86	4.28	3.96	3.24	3.4	4.29	2.98	3.14	0.14
41	3.86	3.74	3.63	3.52	3.36	3.77	3.56	3.51	0.05
42	3.94	3.85	3.69	3.54	3.4	3.9	3.54	3.54	0.05
43	3.95	3.82	3.72	3.62	3.28	3.88	3.6	3.63	0.06
44	4.03	3.93	3.78	3.64	3.33	4.01	3.59	3.65	0.06
45	3.51	3.4	3.27	3.13	3.16	3.34	3.32	3.13	0.04
46	3.59	3.52	3.33	3.16	3.21	3.47	3.27	3.15	0.05
47	3.68	3.56	3.44	3.32	3.18	3.55	3.45	3.3	0.05
48	3.76	3.68	3.5	3.34	3.23	3.68	3.41	3.33	0.06
49	3.89	4.34	3.85	3.4	3.45	4.28	3.38	3.23	0.11
50	3.89	4.38	3.84	3.56	3.62	4.33	3.42	3.45	0.1
51	3.97	4.42	3.93	3.49	3.38	4.38	3.49	3.34	0.12
52	3.97	4.45	3.92	3.66	3.54	4.43	3.53	3.56	0.1
53	3.56	4.03	3.51	3.03	3.27	3.87	2.82	2.86	0.13
54	3.57	4.09	3.51	3.21	3.46	3.94	2.81	3.1	0.12
55	3.71	4.18	3.67	3.2	3.28	4.06	3.12	3.02	0.12
56	3.72	4.22	3.66	3.38	3.46	4.13	3.14	3.25	0.11
57	3.89	3.86	3.5	3.44	3.28	3.78	3.5	3.43	0.06
58	3.96	3.96	3.56	3.46	3.32	3.91	3.47	3.45	0.07
59	3.98	3.94	3.6	3.54	3.21	3.9	3.54	3.55	0.07
60	4.05	4.05	3.65	3.56	3.25	4.02	3.52	3.57	0.08
61	3.53	3.51	3.13	3.04	3.07	3.34	3.27	3.04	0.06
62	3.6	3.62	3.18	3.06	3.11	3.47	3.21	3.06	0.07
63	3.71	3.68	3.31	3.23	3.1	3.56	3.39	3.22	0.07
64	3.78	3.79	3.37	3.25	3.14	3.68	3.35	3.24	0.08
Average	***3.33***								***0.07***

References

[1]J.G. Teng, J.F. Chen, S.T. Smith, L. Lam. **FRP-strengthened RC structures.** John Wiley & Sons (2002)

[2]Y.F. Wu, C. Jiang. **Effect of load eccentricity on the stress-strain relationship of FRP-confined concrete columns.** Compos Struct, 98 (2013), pp. 228-241

[3]C. Jiang, Y.F. Wu, G. Wu. **Plastic hinge length of FRP-confined square RC columns.** J Compos Constr, 18 (4) (2014), p. 04014003

[4]C. Jiang, Y.F. Wu, J.F. Jiang. **Effect of aggregate size on stress-strain behavior of concrete confined by fiber composites.** Compos Struct, 168 (2017), pp. 851-862
[5]X. Li, X.L. Gu, Y. Ouyang, X.B. Song. **Long-term behavior of existing low-strength reinforced concrete beams strengthened with carbon fibre composite sheets.** Compos Part B, 43 (3) (2012), pp. 1637-1644
[6]X. Li, X.L. Gu, X.B. Song, Y. Ouyang, Z.L. Feng. **Contribution of U-shaped strips to the flexural capacity of low-strength reinforced concrete beams strengthened with carbon fibre composite sheets.** Compos Part B, 45 (1) (2013), pp. 117-126
[7]A. Kezmane, S. Boukais, M. Hamizia. **Numerical simulation of squat reinforced concrete wall strengthened by FRP composite material.** Front Struct Civ Eng, 10 (4) (2016), pp. 445-455
[8]A. Zhou, R. Qin, L. Feo, R. Penna, D. Lau. **Investigation on interfacial defect criticality of FRP-bonded concrete beams.** Compos Part B, 113 (2017), pp. 80-90
[9]A. Zhou, O. Büyüköztürk, D. Lau. **Debonding of concrete-epoxy interface under the coupled effect of moisture and sustained load.** Cem Concr Compos, 80 (2017), pp. 287-297
[10]X.L. Zhao. **FRP-strengthened metallic structures.** CRC Press (2013)
[11]Q.Q. Yu, T. Chen, X.L. Gu, X.L. Zhao, Z.G. Xiao. **Fatigue behaviour of CFRP strengthened steel plates with different degrees of damage.** Thin-Walled Struct, 69 (2013), pp. 10-17
[12]P. Feng, L.L. Hu, X.L. Zhao, L. Cheng, S.H. Xu. **Study on thermal effects on fatigue behavior of cracked steel plates strengthened by CFRP sheets.** Thin-Walled Struct, 82 (2014), pp. 311-320
[13]E. Ghafoori, M. Motavalli, X.L. Zhao, A. Nussbaumer, M. Fontana. **Fatigue design criteria for strengthening metallic beams with bonded CFRP plates.** Eng Struct, 101 (2015), pp. 542-557
[14]L.L. Hu, X.L. Zhao, P. Feng. **Fatigue behavior of cracked high-strength steel plates strengthened by CFRP sheets.** J Compos Constr, 20 (6) (2016), p. 04016043
[15]B. Zheng, M. Dawood. **Debonding of carbon fiberreinforced polymer patches from cracked steel elements under fatigue loading.** J Compos Constr, 20 (6) (2016), p. 04016038
[16]Q.Q. Yu, Y.F. Wu. **Fatigue strengthening of cracked steel beams with different configurations and materials.** J Compos Constr, 21 (2) (2017), p. 04016093
[17]D. Van Gemert. **Force transfer in epoxy bonded steel/concrete joints.** Int J Adhes Adhes, 1 (2) (1980), pp. 67-72
[18]P. Holzenkämpfer. **Ingenieur modelle des verbundes geklebter bewehrung für betonbauteile.** [Ph.D. thesis] TU Braunschweig, Germany (1994) [in German]
[19]Y. Hiroyuki, Z.S. Wu. **Analysis of debonding fracture properties of CFS strengthened member subject to tension.** Proc., 3rd Int. Symp. on Non-metallic (FRP) Reinforcement for Concrete Structures, vol. 1, Japan Concrete Institute, Tokyo, Japan (1997)
[20]J.F. Chen, J.G. Teng. **Anchorage strength models for FRP and steel plates bonded to concrete.** J Struct Eng, 127 (7) (2001), pp. 784-791
[21]International Federation for Structural Concrete fib. Externally bonded FRP reinforcement for RC structures. Bulletin 14, Lausanne, Switzerland; 2001.
[22]J.G. Dai, T. Ueda, Y. Sato. **Development of the nonlinear bond stress-slip model of fiber reinforced plastics sheet-concrete interfaces with a simple method.** J Compos Constr, 9 (1) (2005), pp. 52-62
[23]Y.W. Zhou. **Analytical and experimental study on the strength and ductility of FRP-reinforced high strength concrete beam.** [Ph.D. thesis] Dalian Univ. of Technology, Dalian, China (2009) [in Chinese]
[24]Y.F. Wu, C. Jiang. **Quantification of bond-slip relationship for externally bonded FRP-to-concrete joints.** J Compos Constr, 17 (5) (2013), pp. 673-686
[25]K. Nakaba, T. Kanakubo, T. Furuta, H. Yoshizawa. **Bond behavior between fiber-reinforced polymer laminates and concrete.** ACI Struct J, 98 (3) (2001), pp. 359-367
[26]H. Yuan, J.G. Teng, R. Seracino, Z.S. Wu, J. Yao. **Full range behavior of FRP-to-concrete bonded joints.** Eng Struct, 26 (5) (2004), pp. 553-565
[27]H. Yuan, X.S. Lu, D. Hui, L. Feo. **Studies on FRP-concrete interface with hardening and softening bond-slip law.** Compos Struct, 94 (12) (2012), pp. 3781-3792

[28]B. Ferracuti, M. Savoia, C. Mazzotti. **Interface law for FRP–concrete delamination.** Compos Struct, 80 (4) (2007), pp. 523-531
[29]X.Z. Lu, J.G. Teng, L.P. Ye, J.J. Jiang. **Bond-slip models for FRP sheets/plates bonded to concrete.** Eng Struct, 27 (6) (2005), pp. 920-937
[30]Y.W. Zhou, Y.F. Wu. **General model for constitutive relationships of concrete and its composite structures.** Compos Struct, 94 (2) (2012), pp. 580-592
[31]H. Abdel Baky, U.A. Ebead, K.W. Neale. **Nonlinear micromechanics-based bond-slip model for FRP/concrete interfaces.** Eng Struct, 39 (2012), pp. 11-23
[32]Y.F. Wu, X.S. Xu, J.B. Sun, C. Jiang. **Analytical solution for the bond strength of externally bonded reinforcement.** Compos Struct, 94 (11) (2012), pp. 3232-3239
[33]A.S. Nowak, K.R. Collins. **Reliability of Structures.** (2nd ed.), CRC Press (2012)
[34]N. Plevris, T.C. Triantafillou, D. Veneziano. **Reliability of RC members strengthened with CFRP laminates.** J Struct Eng, 121 (7) (1995), pp. 1037-1044
[35]R.A. Atadero, V.M. Karbhari. **Calibration of resistance for reliability based design of externally bonded FRP composites.** Compos Part B, 39 (4) (2008), pp. 665-679
[36]N.Y. Wang, B.R. Ellingwood, A.H. Zureick. **Reliability-based evaluation of flexural members strengthened with externally bonded fiber reinforced polymer composites.** J Struct Eng, 136 (9) (2010), pp. 1151-1160
[37]J.W. Shi, Z.S. Wu, X. Wang, M. Noori. **Reliability analysis of intermediate crack-induced debonding failure in FRP-strengthened concrete members.** Struct Infrastruct E, 11 (12) (2015), pp. 1651-1671
[38]R. Atadero, L. Lee, V.M. Karbhari. **Consideration of material variability in reliability analysis of FRP strengthened bridge decks.** Compos Struct, 70 (4) (2005), pp. 430-443
[39]American Concrete Institute ACI. **Guide for the design and construction of externally bonded FRP systems for strengthening concrete structures.** American Concrete Institute (2008) [ACI 440.2R-08]
[40]American Association of State Highway and Transportation Officials AASHTO. AASHTO LRFD bridge design specifications; 2014.
[41]A.H.S. Ang, W.H. Tang. **Probability concepts in engineering planning and design.** Basic principles, vol. 1, John Wiley & Sons (1975)
[42]D.M. Zhang, K.K. Phoon, H.W. Huang, Q.F. Hu. **Characterization of model uncertainty for cantilever deflections in undrained clay.** J Geotech Geoenviron, 141 (1) (2015), p. 04014088
[43]J. Yao, J.G. Teng, J.F. Chen. **Experimental study on FRP-to-concrete bonded joints.** Compos Part B, 36 (2) (2005), pp. 99-113
[44]Z.S. Wu, H. Yuan, H. Niu. **Stress transfer and fracture propagation in different kinds of adhesive joints.** J Eng Mech, 128 (5) (2002), pp. 562-573
[45]Z.S. Wu, S.M. Islam, H. Said. **A three-parameter bond strength model for FRP-concrete interface.** J Reinf Plast Comp, 28 (19) (2009), pp. 2309-2323
[46]J.P. Lin, Y.F. Wu. **Numerical Analysis of interfacial bond behavior of externally bonded FRP-to-concrete joints.** J Compos Constr, 20 (5) (2016), p. 04016028
[47]Maeda T, Asano Y, Sato Y. A study on bond mechanism of carbon fiber sheet. Non-metallic (FRP) reinforcement for concrete structures. In: Proceedings of the Third International Symposium (FRPRCS-3), Sapporo, Japan; 1997.
[48]B. Täljsten. **Defining anchor lengths of steel and CFRP plates bonded to concrete.** Int. J Adhes Adhes, 17 (4) (1997), pp. 319-327
[49]L. Bizindavyi, K.W. Neale. **Transfer lengths and bond strengths for composites bonded to concrete.** J Compos Constr, 3 (4) (1999), pp. 153-160
[50]Brosens K, Van Gemert D. Anchorage design for externally bonded carbon fiber reinforced polymer laminates. In: Proc., 4th Int. Symp. on fiber reinforced polymer reinforcement for reinforced concrete structures, Farmington Hills, MI; 1999.
[51]A. Kamiharako, T. Shimomura, K. Maruyama, H. Nishida. **Analysis of bond and debonding behavior of continuous fiber sheet bonded on concrete.** J Mater Concr Struct Pavement, 634 (45) (1999), pp. 197-208 [in Japanese]

[52]Z.S. Wu, H. Yuan, H. Yoshizawa, T. Kanakubo. **Experimental/analytical study on interfacial fracture energy and fracture propagation along FRP-concrete interface.** American Concrete Institute, Farmington Hills, MI (2001), pp. 133-152. ACI International SP-201-8

[53]J.G. Dai, Y. Sato, T. Ueda. **Improving the load transfer and effective bond length for FRP composites bonded to concrete.** Proc Jap Concr Inst, 24 (2) (2002), pp. 1423-1428

[54]J.G. Dai. **Interfacial models for fiber reinforced polymer (FRP) sheets externally bonded to concrete.** [Ph.D. thesis]. Hokkaido Univ., Hokkaido, Japan (2003)

[55]Zhao M, Ansari F. Bond properties of FRP fabrics and concrete joints. Proc., 13th World Conf. on Earthquake Engineering-13 WCEE, Vancouver, Canada; 2004.

[56]Mazzotti C, Ferracuti B, Savoia M. FRP-concrete delamination results adopting different experimental pure shear set-ups. Proc., 11th Int. Conf. on Fracture-ICF 11, Turin, Italy; 2005.

[57]S.K. Sharma, M.S. Mohamed Ali, D. Goldar, P.K. Sikdar. **Plate-concrete interfacial bond strength of FRP and metallic plated concrete specimens.** Compos Part B, 37 (1) (2006), pp. 54-63

[58]H. Toutanji, P. Saxena, L. Zhao, T. Ooi. **Prediction of interfacial bond failure of FRP-concrete surface.** J Compos Constr, 11 (4) (2007), pp. 427-436

[59]M. Leone, S. Matthys, M.A. Aiello. **Effect of elevated service temperature on bond between FRP EBR systems and concrete.** Compos Part B, 40 (1) (2009), pp. 85-93

[60]F. Ceroni, M. Pecce. **Evaluation of bond strength in concrete elements externally reinforced with CFRP sheets and anchoring devices.** J Compos Constr, 14 (5) (2010), pp. 521-530

[61]J.W. Shi, H. Zhu, Z.S. Wu, G. Wu. **Experimental study on bond behavior between Basalt/Hybrid FRP sheets and concrete substrates.** J Southeast Univ, 40 (3) (2010), pp. 554-558 [in Chinese]

[62]A. Bilotta, F. Ceroni, M. Di Ludovico, E. Nigro, M. Pecce, G. Manfredi. **Bond efficiency of EBR and NSM FRP systems for strengthening concrete members.** J Compos Constr, 15 (5) (2011), pp. 757-772

[63]L. Biolzi, C. Ghittoni, R. Fedele, G. Rosati. **Experimental and theoretical issues in FRP-concrete bonding.** Constr Build Mater, 41 (2013), pp. 182-190

[64]H.M. Diab, O.A. Farghal. **Bond strength and effective bond length of FRP sheets/plates bonded to concrete considering the type of adhesive layer.** Compos Part B, 58 (2014), pp. 618-624

[65]A. Hosseini, D. Mostofinejad. **Effective bond length of FRP-to-concrete adhesively-bonded joints: experimental evaluation of existing models.** Int J Adhes Adhes, 48 (2014), pp. 150-158

[66]H. Ko, S. Matthys, A. Palmieri, Y. Sato. **Development of a simplified bond stress-slip model for bonded FRP-concrete interfaces.** Constr Build Mater, 68 (2014), pp. 142-157

[67]P. Zhang, G. Wu, H. Zhu, S.P. Meng, Z.S. Wu. **Mechanical performance of the wet-bond interface between FRP plates and cast-in-place concrete.** J Compos Constr, 18 (6) (2014), p. 04014016

[68]R. Kalfat, R. Al-Mahaidi. **Development of a hybrid anchor to improve the bond performance of multiple plies of FRP laminates bonded to concrete.** Constr Build Mater, 94 (2015), pp. 280-289

[69]T. Mohammadi, B.L. Wan. **Sensitivity analysis of stress state and bond strength of fiber-reinforced polymer/concrete interface to boundary conditions in single shear pull-out test.** Adv Mech Eng, 7 (5) (2015), pp. 1-11

[70]Y.F. Pan, G.J. Xian, M.A.G. Silva. **Effects of water immersion on the bond behavior between CFRP plates and concrete substrate.** Constr Build Mater, 101 (2015), pp. 326-337

[71]Y.W. Zhou, Z.H. Fan, J. Du, L.L. Sui, F. Xing. **Bond behavior of FRP-to-concrete interface under sulfate attack: An experimental study and modeling of bond degradation.** Constr Build Mater, 85 (2015), pp. 9-21

[72]F. Ceroni, M. Ianniciello, M. Pecce. **Bond behavior of FRP carbon plates externally bonded over steel and concrete elements: Experimental outcomes and numerical investigations.** Compos Part B, 92 (2016), pp. 434-446

[73]M.J. Chajes, W.W. Finch, T.F. Januszka, T.A. Thomson. **Bond and force transfer of composite-material plates bonded to concrete.** ACI Struct J, 93 (2) (1996), pp. 208-217

[74]K. Takeo, H. Matsushita, T. Makizumi, G. Nagashima. **Bond characteristics of CFRP sheets in the CFRP bonding technique.** Proc Jap Concr Inst, 19 (2) (1997), pp. 1599-1604

[75]Y. Sato, Y. Asano, T. Ueda. **Fundamental study on bond mechanism of carbon fiber sheet.** Proc Jpn Soc Civ Eng, 648 (2000), pp. 71-87. [in Japanese]
[76]Ebead UA, Neale KW, Bizindavyi L. On the interfacial mechanics of FRP-strengthened concrete structures. In: Proc., 2nd Int. Conf. on FRP Composites in Civil Engineering-CICE2004, Adelaide, Australian; 2004.
[77]Pham H, Al-Mahaidi R. Bond characteristics of CFRP fabrics bonded to concrete members using wet lay-up method. In: Proc., 2nd Int. Conf. on FRP composites in civil engineering-CICE 2004; 2004.
[78]H. Zhu, G. Wu, J.W. Shi, C. Liu, X.Y. He. **Digital image correlation measurement of the bond-slip relationship between fiber-reinforced polymer sheets and concrete substrate.** J Reinf Plast Comp, 33 (17) (2014), pp. 1590-1603
[79]K.K. Phoon, F.H. Kulhawy. **Characterisation of model uncertainties for laterally loaded rigid drilled shafts.** Géotechnique, 55 (1) (2005), pp. 45-54
[80]Joint Committee on Structural Safety JCSS. JCSS probabilistic model code. ISBN 978-3-909386-79-6, Zurich, Switzerland; 2011.
[81]G.T.C. Kung, C.H. Juang, E.C.L. Hsiao, Y.M.A. Hashash. **Simplified model for wall deflection and ground-surface settlement caused by braced excavation in clays.** J Geotech Geoenviron Eng, 133 (2007), pp. 731-747
[82]C. Tang, K.K. Phoon. **Model uncertainty for predicting the bearing capacity of sand overlying clay.** Int. J. Geomech., 17 (7) (2017), p. 04017015
[83]American Society of Civil Engineers ASCE. Minimum design loads for buildings and other structures. ASCE/SEI 7-10; 2010.
[84]D.V. Val. **Reliability of fiber-reinforced polymer-confined reinforced concrete columns.** J Struct Eng, 129 (8) (2003), pp. 1122-1130
[85]T. Allen, A.S. Nowak, R.J. Bathurst. **Calibration to determine load and resistance factors for geotechnical and structural design. Transportation research circular E-C079.** Transportation Research Board (2005)
[86]American Association of State Highway and Transportation Officials AASHTO. Manual for condition evaluation and load and resistance factor rating (LRFR) of Highway Bridges; 2011.
[87]A.M. Okeil, A. Belarbi, D.A. Kuchma. **Reliability assessment of FRP-strengthened concrete bridge girders in shear.** J Compos Constr, 17 (1) (2013), pp. 91-100
[88]A.S. Nowak, M.M. Szerszen. **Calibration of design code for buildings (ACI 318): Part 1-statistical models for resistance.** ACI Struct J, 100 (3) (2003), pp. 377-382
[89]T.V. Galambos, B. Ellingwood, J.G. MacGregor, Cornell C. Allin. **Probability based load criteria: assessment of current design practice.** J Struct Div, 108 (5) (1982), pp. 959-977
[90]A.M. Hasofer, N.C. Lind. **Exact and invariant second-moment code format.** J Eng Mech Divis, 100 (1) (1974), pp. 111-121
[91]B.K. Low, W.H. Tang. **Efficient reliability evaluation using spreadsheet.** J Eng Mech, 123 (7) (1997), pp. 749-752
[92]M. Rosenblatt. **Remarks on a multivariate transformation.** Ann Math Stat, 23 (3) (1952), pp. 470-472
[93]N.Y. Wang, B.R. Ellingwood. **Limit state design criteria for FRP strengthening of RC bridge components.** Struct Saf, 56 (2015), pp. 1-8
[94]M. Israel, B. Ellingwood, R. Corotis. **Reliability-based code formulations for reinforced concrete buildings.** J Struct Eng, 113 (10) (1987), pp. 2235-2252